

# The Southern 2MASS AGN Survey: spectroscopic follow-up with 6dF

Frank J. Masci and Roc M. Cutri

Infrared Processing and Analysis Center, Caltech 100-22, Pasadena, CA 91125, USA

`fmasci@caltech.edu`

Paul J. Francis

Australian National University, ACT 0200, Australia

Brant O. Nelson<sup>1</sup>

Infrared Processing and Analysis Center, Caltech 100-22, Pasadena, CA 91125, USA

John P. Huchra

Harvard-Smithsonian Center for Astrophysics, Cambridge, MA 02138, USA

and

D. Heath Jones, Matthew Colless, and Will Saunders

Anglo-Australian Observatory, P.O. Box 296, Epping, NSW 1710, Australia

Received \_\_\_\_\_; accepted \_\_\_\_\_

v.5, To appear in PASA

---

<sup>1</sup>present address: Vermont Academy, Saxtons River, VT 05154, USA

## ABSTRACT

The Two Micron All-Sky Survey (2MASS) has provided a uniform photometric catalog to search for previously unknown red AGN and QSOs. We have extended the search to the southern equatorial sky by obtaining spectra for 1182 AGN candidates using the Six Degree Field (6dF) multifibre spectrograph on the UK Schmidt Telescope. These were scheduled as auxiliary targets for the 6dF Galaxy Redshift Survey. The candidates were selected using a single color cut of  $J - K_s > 2$  to  $K_s \lesssim 15.5$  and a galactic latitude of  $|b| > 30^\circ$ . 432 spectra were of sufficient quality to enable a reliable classification. 116 sources (or  $\simeq 27\%$ ) were securely classified as type 1 AGN, 20 as probable type 1s, and 57 as probable type 2 AGN. Most of them span the redshift range  $0.05 < z < 0.5$  and only 8 (or  $\sim 6\%$ ) were previously identified as AGN or QSOs. Our selection leads to a significantly higher AGN identification rate amongst local galaxies ( $> 20\%$ ) than in any previous (mostly blue-selected) galaxy survey. A small fraction of the type 1 AGN could have their optical colors reddened by optically thin dust with  $A_V < 2$  mag relative to optically selected QSOs. A handful show evidence for excess far-IR emission. The equivalent width (EW) and color distributions of the type 1 and 2 AGN are consistent with AGN unified models. In particular, the EW of the [O III] emission line weakly correlates with optical–near-IR color in each class of AGN, suggesting anisotropic obscuration of the AGN continuum. Overall, the optical properties of the 2MASS red AGN are not dramatically different from those of optically-selected QSOs. Our near-IR selection appears to detect the most near-IR luminous QSOs in the local universe to  $z \simeq 0.6$  and provides incentive to extend the search to deeper near-IR surveys.

*Subject headings:* galaxies: active — quasars: general — infrared: general — surveys

## 1. Introduction

Much of our knowledge about the distribution and properties of Active Galactic Nuclei (AGN) has come from samples that are flux-limited at blue optical wavelengths. This is because their spectral energy distributions (SEDs) generally exhibit a UV flux excess. Such surveys can be very efficient and complete down to their blue flux limit, for example, the Large Bright Quasar Survey (LBQS; Hewett et al. 1995). However, any survey with a blue-flux limit will be relatively biased against objects whose intrinsic emission peaks at other wavelengths, e.g., near-IR emission from the host galaxy (Masci et al. 1998; Benn et al. 1998). Alternatively, the optical/UV can be partially or heavily absorbed by dust, as revealed by radio, near-to-mid infrared, and X-ray surveys (Webster et al. 1995; Gregg et al. 2002; Polletta et al. 2007; Donley et al. 2008). The Sloan Digital Sky Survey (SDSS; Richards et al. 2002) has employed a range of multicolor optical selection techniques with relaxed constraints on morphology to search for QSOs to redshifts of  $\simeq 6$ . This has reduced the bias relative to the simple UV-excess criteria used in early surveys, but has not eliminated it.

A complete census of AGN over cosmic time is essential for understanding galaxy formation and evolution since the properties of the central black hole and host galaxy are intimately linked (see reviews in Ho 2004). The fraction of AGN missing from optically selected samples, both as a function of redshift and luminosity is an important parameter. This is expected to be related to the duty cycle of black-hole fueling and timescales for regulating star formation. Values are currently very uncertain and range from 15 to over 50% (e.g., Richards et al. 2003; Brown et al. 2006; Glikman et al. 2004, 2007). This uncertainty is due to selection of the appropriate comparison sample of optically selected AGN, properties of the “unbiased” sample and how representative it is, and difficulties in quantifying the amount of bias (e.g., dust extinction).

### 1.1. Near-IR Selection

Warren et al. (2000) showed that it is possible to construct a complete  $K$ -band-limited QSO sample by combining optical and near-IR photometry. This exploits the characteristic  $K$ -band excess seen in QSOs compared to stars and has been termed the KX-selection method. A number of small pilot surveys have employed KX-selection and variants thereof (e.g., Croom et al. 2001; Sharp et al. 2002; Jurek et al. 2008; Smail et al. 2008). The largest is being compiled from the UKIDSS Large Area Survey covering  $12.8 \text{ deg}^2$  (Maddox et al. 2008). This survey currently reports a surface density of  $\simeq 15 \text{ deg}^{-2}$  for broad-lined AGN with  $K \leq 17$  and  $z < 3$ . They estimated that about 50% were missed by SDSS, therefore revealing a large population of red QSOs.

Although the KX method is turning up many luminous red QSOs to high redshift, the situation is different for less luminous local AGN (e.g., Seyfert nuclei). These are usually not found by color selection since host galaxy light can dominate their broadband colors. Historically, they are found by taking optical spectra of the nuclear regions of large samples of galaxies (e.g., Ho et al. 1997). Many of these samples are flux-limited at blue optical wavelengths and hence subject to bias. The most significant bias is that the blue light is dominated by recent star formation which overwhelms any emission from a central AGN. A near-IR selected sample of local galaxies using color criteria analogous to that used in KX methods will reduce this bias (see below).

The largest near-IR survey to date is the Two Micron All Sky Survey (2MASS; Skrutskie et al. 2006). There have been several studies that searched for AGN in 2MASS. The first was that from Cutri et al. (2002) in the northern equatorial sky. They selected sources with  $J - K_s > 2$  and  $K_s \leq 15.5^1$  at galactic latitude  $|b| > 30 \text{ deg}$ . Spectroscopic

---

<sup>1</sup> $K_s$  is similar to the  $K$  filter but cutting off at a shorter red wavelength to minimize

follow-up revealed that  $\sim 75\%$  were previously unidentified AGN, with  $\sim 80\%$  of these associated with broad emission-line (type 1) AGN, i.e., Seyfert 1s and QSOs, and the remainder were narrow-line (type 2) AGN, typically Seyfert 2s, type 2 QSOs and liners. They spanned a redshift range of  $0.03 < z < 2.52$  with a median of  $\sim 0.22$ , therefore, the AGN were predominately local. The extrapolated surface density of all AGN types was  $\sim 0.57 \text{ deg}^{-2}$  and is significantly higher than that of optically selected AGN at the same  $K_s$  magnitude. A significant fraction also showed unusually high polarization properties (Smith et al. 2002) and very weak X-ray emission (Wilkes et al. 2002).

Other 2MASS studies involved cross-correlating with the FIRST radio catalog (Gregg et al. 2002; Glikman et al. 2007). These turned up a number of extremely red QSOs at high redshift, some showing strong evidence for dust. Barkhouse & Hall (2001) studied the 2MASS colors of QSOs identified at other wavelengths, primarily from the Veron-Cetty & Veron (2000) catalog, and Georgakakis et al. (2009) used mid and far IR observations of red 2MASS AGN to infer their relationship to Luminous IR Galaxies (LIRGs). Most of these studies however used single band 2MASS detections (in  $J$ ,  $H$  or  $K_s$ ) and therefore could have missed many red AGN. Furthermore, none were able to provide a census of AGN in the 2MASS catalog.

A uniform unbiased survey of 2MASS AGN was carried out by Francis et al. (2004) by selecting candidates in the southern hemisphere covering  $12.56 \text{ deg}^2$  using a moderate color cut of  $J - K_s > 1.2$ . This color cut significantly reduced contamination from foreground stars. Spectroscopic follow-up revealed that  $\sim 1.2\%$  were broad-line AGN and  $\sim 4\%$  were galaxies with Seyfert 2 nuclei. The main findings were that: (i) the type 1 AGN are predominately at low redshifts ( $z < 0.3$ ) and contamination from host galaxy light would make them hard to find in optically selected QSO samples (e.g., the SDSS); (ii)

---

thermal emission.

the incidence of type 2 AGN amongst local galaxies is higher than usual when compared to blue-selected galaxy samples. The results of this study are complementary to those presented here and will be discussed in more detail later.

The above studies indicate that 2MASS is sensitive to the local AGN population. The luminosity of broad-lined QSOs in particular in the local universe is only slightly greater than that of their host galaxies (e.g., Hao & Strauss 2004). Only a small amount of dust extinction is needed to mis-identify them or turn them into type 2 AGN. This is in contrast to the heavily obscured, high-luminosity, and usually unresolved QSOs at high redshift. Therefore, even though near-IR color-selected surveys are less biased than those in the optical/UV, they are still somewhat biased against the reddest QSOs. They do however have the advantage that candidates selected in the near-IR will be bright enough to allow spectroscopic followup with relative ease.

It is worth mentioning why a red  $J - K_s$  color cut has proven so efficient at finding AGN in the relatively shallow 2MASS Point Source Catalog (PSC). There are three reasons. First, contamination from halo giant and disk dwarf stars is very much eliminated, where the majority have  $J - K_s \lesssim 0.75$  (Francis et al. 2004). Second, the 2MASS colors of galaxies are predominately blue, with a median  $J - K_s \sim 1.1$  at  $z \lesssim 0.1$  and a  $1-\sigma$  upper limit of  $J - K_s < 1.6$  at  $z \simeq 0.2$  (Jarrett et al. 2000; Jarrett 2004). This color reddens rapidly for galaxies at higher redshifts due to the  $k$ -correction, approaching  $J - K_s \simeq 2$  at  $z \sim 0.4$ . However, typical  $L^*$  galaxies at such redshifts will be well below the detection limit of the 2MASS PSC. Contamination from non-active galaxies is therefore expected to be small overall.

The third reason is motivated by the fact that an extremal color cut of  $J - K_s > 2$  has been shown to discriminate red AGN from UV/optically-selected ones in large samples of known AGN (Barkhouse & Hall 2001; Cutri et al. 2002). For example, 2MASS detects a

large fraction ( $\sim 75\%$ ) of the LBQS QSOs in all three near-IR bands ( $J$ ,  $H$  or  $K_s$ ). Most of these have  $J - K_s < 2$ . Therefore,  $J - K_s > 2$  isolates the reddest subset of the optically selected population and is likely to probe many more. It is also interesting to note that nearly all known QSOs at  $z \lesssim 0.5$  have  $J - K_s > 1.2$  (Francis et al. 2000; Barkhouse & Hall 2001).

In this paper, we extend the work of Cutri et al. (2002) and Francis et al. (2004) to search for additional red 2MASS AGN in the southern equatorial sky. We assembled a relatively unbiased sample of red AGN candidates using a color cut of  $J - K_s > 2$  on the 2MASS Point Source Working Database and then used the brute-force capabilities of the Six Degree Field (6dF) multiobject spectrograph to obtain spectra of a subsample. We utilized the efficient mapping strategy of the 6dF Galaxy Survey (6dFGS) with our candidates selected as secondary targets in the program.

Our sample and target selection are described in Section 2. Observations and data reduction are described in Section 3, and spectral classifications in Section 4. Properties of the newly discovered AGN and comparisons to optically selected QSO samples are discussed in Section 5. Conclusions are given in Section 6. We assume a concordance cosmology with  $H_0 = 70 \text{ km s}^{-1} \text{ Mpc}^{-1}$ ,  $\Omega_m = 0.3$ , and  $\Omega_\Lambda = 0.7$ . All magnitudes, unless otherwise specified, are based on the Vega system.

## 2. Sample and Target Selection

Candidates were initially selected from the 2MASS Point Source Working Database using the following criteria: a color cut of  $J - K_s > 2$ ;  $K_s \leq 15.5$ ; detections in all three bands ( $J$ ,  $H$  and  $K_s$ ); galactic latitude  $|b| > 30^\circ$ ; and excluding a region of  $\sim 170 \text{ deg}^2$  covering the Large and Small Magellanic Clouds. Previously identified sources were not

omitted. This yielded 16,977 candidates in an effective area of  $\sim 20,400 \text{ deg}^2$  over the whole sky. These criteria define the “master” catalog of red AGN candidates, and were used in northern hemisphere follow-up studies by Cutri et al. (2002).

Note that a detection in the H-band was included for reliability. The red AGN candidate selection criteria were originally devised during the early stages of the survey before many of the source quality metrics were mature. Sources detected in all three survey bands were known to be of the highest reliability. Therefore, three-band detection was included with the two-band color limit to minimize sample contamination by spurious sources with unusual colors.

Southern equatorial ( $\delta < 0^\circ$ ) AGN candidates from the master catalog were then position matched against the SuperCOSMOS Sky Survey database (Hambly et al. 2001a). A match radius of 4 arcsec was used and no optical magnitude cut was initially imposed.  $\simeq 0.7\%$  of matches resulted in multiple (ambiguous) associations and were excluded. This yielded 6386 matches with an overall position-difference dispersion of  $\sigma \simeq 0.6 \text{ arcsec}$ . A sample of 2260 candidates was then compiled by selecting sources with SuperCOSMOS magnitudes of  $b_J \leq 18$  and  $r_F \leq 17$ . These limits were required to obtain good signal-to-noise ratio spectra ( $S/N \gtrsim 10/\text{pixel}$ ) and enable reliable identifications. The reliability of the SuperCOSMOS optical detections to these magnitude limits is expected to be  $> 99.9\%$  (Hambly et al. 2001b). The single  $b_J$  and  $r_F$  band photometry has an accuracy of  $\sigma \sim 0.3 \text{ mag}$  while due to specifics of the calibration procedure,  $b_J - r_F$  colors are expected to have an accuracy of  $\sigma \lesssim 0.12 \text{ mag}$  (for details, see Hambly et al. 2001b). The 2260 candidates were then proposed for follow-up with the 6dF multifibre spectrograph. 1182 were eventually allocated fibers, mainly as secondary targets during scheduling of observations for the 6dFGS (Jones et al. 2004). Our objects were distributed over an effective non-contiguous area of  $\sim 1592 \text{ deg}^2$ .



It’s important to note that our initial sample of candidates (with  $J - K_s > 2$ ) was selected from an early version of the 2MASS Point Source Working Database. Subsequent recalibration and selection of alternate observations of some of these sources for inclusion in the final 2MASS PSC resulted in some of them having colors  $J - K_s < 2$ . In the end, the majority of sources classified as AGN had  $J - K_s \gtrsim 1.5$ , with  $\sim 20\%$  satisfying  $1.5 \leq J - K_s \leq 2$  according to photometry in the public-release PSC. Uncertainties in the  $J - K_s$  colors were typically  $\lesssim 0.16$  mag ( $1-\sigma$ ).

### 3. Observations and Reduction

Spectra were obtained over the course of the 6dFGS during 2001-2006 using the UK Schmidt Telescope and the 6dF spectrograph (Watson et al. 1998; Saunders et al. 2001). For details on the 6dFGS observing strategy, see Jones et al. (2004, 2009). The primary sample for the 6dFGS was drawn from the 2MASS Extended Source Catalog (XSC; Jarrett et al. 2000). Seventeen additional (secondary) extragalactic samples were merged with the primary sample (see Table 3 in Jones et al. 2009). During survey design, these were given priority indices and our initial sample of 2260 candidates had a completeness in coverage of 91.7%. This gave  $\sim 6$  AGN candidates per 6dF field on average, although not all 6dFGS fields contained our targets because of the different galactic latitude constraints.

The 6dF multifiber spectrograph was able to record up to 120 simultaneous spectra over a  $5.7^\circ$  field. Each fiber has a projected diameter of 6.7 arcsec on the sky. The 2MASS positions were accurate to  $\leq 0.5$  arcsec and therefore light losses due to fiber positioning errors were expected to be small. For the  $10^{th}$ – $90^{th}$  percentile range in redshift for the extragalactic identifications,  $z \simeq 0.15$ – $0.45$ , the fiber diameter corresponds to physical scales of  $R \simeq 17.5$  to  $38.7$  kpc  $h_{70}^{-1}$ . This means the 6dF spectra sampled light from entire galaxies, and not necessarily their nuclei.

Each spectrum was taken using V and R gratings, whose outputs were later spliced to cover the effective wavelength range:  $\sim 3900\text{--}7500\text{\AA}$ . The observed  $S/N$  was typically 3–10  $\text{pixel}^{-1}$ , with  $> 10 \text{ pixel}^{-1}$  being nominal given the brightness of our sources. Spectra with low  $S/N$  were primarily due to poor observing conditions. The spectral resolution was typically  $R \sim 1000$  throughout, corresponding to emission-line Full Width at Half Maxima (FWHM) of  $\sim 4\text{--}8\text{\AA}$  over the observed wavelength range. This enabled us to resolve rest-frame velocities of  $\gtrsim 205 \text{ km s}^{-1}$  over the range  $z \simeq 0.15\text{--}0.45$ , sufficient for AGN identification and classification.

EDITOR: PLACE FIGURE 1 HERE.

The data were reduced, spectra extracted, and wavelength calibrated using a modified version of the 2dFDR package developed for the 2dF Galaxy Redshift Survey. Details of the reduction are described in Jones et al. (2004) and products from the final data release (DR3; April 2009) are described in Jones et al. (2009). The flux calibration was very crude in that the same average spectral transfer function (derived once using a couple of standards) was assumed for every 6dF observation for all time. The spectra are therefore not of spectrophotometric quality. This severely limited our classification process, e.g., using emission line ratios (Section 4). The spectra were corrected for atmospheric absorption and emission features. However in some cases, imperfect sky-subtraction has left the imprint of the brightest sky lines.

Quality flags were assigned by the semi-automated 6dFGS redshift determination pipeline (see Section 4 for details). Almost all redshifts were visually inspected by the 6dFGS team. Quality flags in the range  $Q = 1\text{--}4$  were assigned in the final public catalog<sup>2</sup>.

---

<sup>2</sup>accessed via <http://www.aao.gov.au/6dFGS/>

$Q = 4$  represents a very reliable redshift where typically the median spectral  $S/N$  was  $\sim 10 \text{ pixel}^{-1}$ .  $Q = 3$  was assigned to “likely” redshift and  $Q = 2$  to tentative redshift with spectra warranting further examination. We visually examined all spectra with quality flags  $Q \geq 2$ , although the majority of usable spectra had  $Q = 4$  and a handful had  $Q = 3$ . Due to the faintness of the sources in general, 750 of the 1182 spectra observed were of such poor quality that no classification was possible. Classifications were therefore secured for 432 spectra.

Figure 1 shows the number of proposed AGN candidates (using the optical/near-IR constraints defined in Section 2), the number of 6dF spectra observed, and the number with secure spectral identifications as a function of  $K_s$  magnitude. The dearth of candidates in the faintest bin,  $15 < K_s < 15.5$  is due to a combination of our optical magnitude limits (see below) and the original  $J - K_s > 2$  cutoff. This cutoff implies  $J \gtrsim 17$  for  $K_s > 15$  and hence a fraction of sources are expected to fall below the  $J$ -band flux limit and excluded from the candidate list. This drop was also seen in the Cutri et al. (2002) sample of 704 candidates *with* follow-up optical spectroscopy. Figure 2 shows that we are not significantly biased against identifying sources with the reddest  $J - K_s$  colors. In fact, the spectral identification rate as a function of  $J - K_s$  is approximately uniform.

Figure 1 shows that the number of spectra observed uniformly samples the  $K_s$  distribution of candidates, i.e., the completeness is approximately uniform. However, there is relatively higher incompleteness in the number of spectra *identified* at the faintest magnitudes:  $14.5 < K_s < 15.25$ . The incompleteness in this range is  $\sim 70\%$  with respect to the number of spectra observed. This is primarily due to the faintest sources generally having poorer quality spectra. These are expected to be near the optical magnitude limit imposed for spectroscopy:  $17 \lesssim b_J \leq 18$ . In fact, the introduction of an optical magnitude cut is expected to have biased the spectral sample towards bluer optical colors

in general. Comparing the relative deficit in the number of faint ( $K_s > 14.5$ ) sources to the original candidate  $K_s$  distribution (from Cutri et al. 2002) with no optical magnitude limit imposed, we estimate we have lost  $\gtrsim 35\%$  of candidates due to this optical cut. A majority of these missed candidates (with  $b_J > 18$ ) have  $b_J - K_s$  colors  $\simeq 4 - 6$ . However, the *spectrally*-observed  $b_J - K_s$  distribution (Figure 3) shows that we are not completely biased against identifying the reddest sources. When compared to the colors of optically selected QSOs, the 2MASS AGN have a tail extending to moderately redder colors (see Figure 10 and Section 5.2 for more details).

EDITOR: PLACE FIGURE 2 HERE.

EDITOR: PLACE FIGURE 3 HERE.

#### 4. Classification

All spectra were initially classified using the semi-automated 6dFGS classification software, whose primary purpose was to determine accurate redshifts. This is a modified version of the RUNZ software used for the 2dF Galaxy Redshift Survey (Colless et al. 2001). It used 13 spectral templates to identify spectra using line-fitting and cross-correlation techniques. This program produced very reliable redshifts for all galaxies in general, although was less reliable at separating out the various AGN classes from late and early type galaxies, and stars. All spectra were visually inspected to determine whether a poor-quality spectrum flagged by the 6dFGS software was worthy of further examination.

432 spectra were of sufficient quality to enable a classification of some sort, but not necessarily an unambiguous identification. All spectra were shifted to their rest-frame using redshifts determined by the 6dFGS program.

#### 4.1. Emission-Line Diagnostics

We assembled a database of emission-line diagnostics for all the good quality spectra to assist with the identifications. The diagnostics included line fluxes, equivalent widths (EWs), and dispersion velocities. These were estimated by fitting Voigt profiles and the underlying continua were approximated by linearly interpolating straight-line fits on either side of each line. Line fluxes were then determined by integrating the flux in the fitted profiles above the continuum level. Dispersion velocities were determined from the FWHM of the lines. The lines of interest and the effective wavelength regions used to define the continuum and line integration limits are shown in Table 1.

EDITOR: PLACE TABLE 1 HERE.

The *fitprofs* task in IRAF was used for the automated measurement of line diagnostics. This included the ability to deblend closely separated lines, e.g., H $\alpha$  and [N II]. An important input parameter for the *fitprofs* task is an estimate of the 1-sigma uncertainty per pixel. This allows the program to compute uncertainties in each of the fitted line parameters. Since the fitting was non-linear, this was accomplished using a Monte Carlo simulation. The spectral uncertainty was computed by first selecting a relatively clean region in the rest frame common to each spectrum, i.e., devoid of strong emission and absorption lines. We selected the rest wavelength range 5050–5400Å. We then fitted a straight line to the data in this region using a robust (outlier-resistant) regression method based on the general concept of “M-estimation” (Huber 1981). The uncertainty was then estimated using the median absolute deviation in the residuals from the fit, and is also robust against potential outliers:

$$\sigma \simeq 1.4826 \text{ median } \{|p_i - \text{fit}\{p_i\}|\}, \quad (1)$$

where  $p_i$  is the value of the  $i^{\text{th}}$  pixel in the 1-D spectrum and  $fit\{p_i\}$  is the fitted value. This quantity is scaled such that it converges to the standard-deviation of a Gaussian in the limit of a large sample. For spectra where the range 5050–5400Å included or fell outside the long wavelength end ( $\lambda_{red}$ ) after shifting to the rest frame, a wavelength range of  $\lambda_{red} - 250 \leq \lambda \leq \lambda_{red} - 20\text{Å}$  was used instead. In all cases, this ensured  $> 20$  pixels for the noise computation.

We estimated the smallest EW we are sensitive to by examining the dispersion in H $\alpha$  and H $\beta$  EWs of all the galaxies (and potential AGN) with the best quality spectra ( $Q = 4$ ). Figure 4 shows these distributions. EW measurements clustered around zero are lineless galaxies where an identification would be highly unreliable, if at all possible. We find we should be sensitive to galaxies with rest frame EW in either H $\alpha$  or H $\beta$  of  $\gtrsim 5\text{Å}$ . Given our observed wavelength range, either of these lines are expected to be observed at  $z \lesssim 0.5$  and therefore were used as constraints in the identification process below.

EDITOR: PLACE FIGURE 4 HERE.

Line fluxes and EWs were also measured interactively by integrating the line fluxes directly from the 1-D spectra. These were in excellent agreement, to within measurement error, with the profile-derived fluxes from above. All lines were visually inspected and unreliable flux measurements flagged. These were primarily lines that were contaminated by a strong sky line or atmospheric absorption band. Our final emission line database retained lines with fluxes  $\gtrsim 2.5\sigma$ , and lines that were clearly discernable by eye in case our automated measurement of  $\sigma$  was overestimated. Unreliable  $\sigma$  estimates occurred in  $\simeq 7\%$  of the spectra. Note that we did not correct the emission line fluxes for any underlying absorption (e.g., from stellar photospheres) since a study using similar spectra from 2dF by Francis et al. (2004) found this effect to be negligible.

A first pass examination of the spectra together with initial classifications provided by the 6dFGS program motivated us to define six broad object classes: type 1 AGN; type 2 AGN; starburst or late-type star forming galaxies; early type galaxies; stars; and unknown emission line galaxies. These classes and the criteria used to identify them are as follows.

Spectra with broad  $H\alpha$  and/or  $H\beta$  emission lines exceeding  $1000 \text{ km s}^{-1}$  (FWHM), or with other broad permitted lines present, e.g.,  $C \text{ III}]$  or  $Mg \text{ II}$  for  $z \gtrsim 1$  and  $z \gtrsim 0.4$  respectively, were classified as type 1 AGN. Included in this criterion are  $S/N \geq 2.5$  on the FWHM measurement and a  $H\alpha$  or  $H\beta$   $EW > 5\text{\AA}$ . Spectra in which known broad lines could be discerned by eye but were relatively noisy, i.e., with flux  $S/N < 2.5$  were classified as “probable” type 1 AGN.

Non-type 1 AGN spectra were classified using line ratios involving good measurements in either of the following line pairs: ( $[O \text{ III}]$ ,  $H\beta$ ) or ( $[N \text{ II}]$ ,  $H\alpha$ ) or ( $[S \text{ II}]$ ,  $H\alpha$ ) or ( $[O \text{ III}]$ ,  $[O \text{ II}]$ ). We first attempted a classification using the diagnostic diagrams of Kewley et al. (2001, 2006), which are based on the classic BPT diagrams of Baldwin et al. (1981). Figures 5 and 6 show the traditional line-ratio diagrams using our good quality spectra (with pre-classified type 1 AGN removed) and where *all* four lines had flux  $S/N \geq 2.5$ . Unfortunately, all four lines in either Figure 5 or 6 were only simultaneously visible (and with good  $S/N$ ) in  $\simeq 8\%$  (23/296) of the good-quality non-type 1 spectra. Furthermore, the errors in the line ratios ( $\simeq 0.2$  dex,  $1-\sigma$ ) were too large for the bulk of these spectra to be reliably classified. We therefore declared the few type 2 AGN and star-forming galaxies that could be classified using this method (at distances  $\geq 1-\sigma$  from the classification boundaries) to be probable identifications.

EDITOR: PLACE FIGURE 5 HERE.

EDITOR: PLACE FIGURE 6 HERE.

For the remaining 273 sources with good quality data and where only one of the above line pairs was available (predominately when  $z \gtrsim 0.1$ ), a galaxy was classified as a “probable” type 2 AGN if either of the following was satisfied:  $\log([\text{O III}]/\text{H}\beta) > 0.3$  or  $\log([\text{N II}]/\text{H}\alpha) > -0.2$  or  $\log([\text{S II}]/\text{H}\alpha) > -0.35$  (e.g., Zakamska et al. 2003) or  $\log([\text{O III}]/[\text{O II}]) > 0$  (e.g., Fraquelli & Storchi-Bergmann 2004; Kewley et al. 2006). Combined with any of these, we also required a rest frame  $\text{FWHM}([\text{O III}]) > 300 \text{ km s}^{-1}$ ,  $\text{FWHM}(\text{H}\alpha \text{ or } \text{H}\beta) < 1000 \text{ km s}^{-1}$ , and  $\text{H}\alpha \text{ or } \text{H}\beta \text{ EW} > 5\text{\AA}$ . The  $\text{FWHM}([\text{O III}])$  limit was included to improve the reliability of type 2 identifications when only one line pair was available. For comparison, Zakamska et al. (2003) assumed  $\text{FWHM}([\text{O III}]) > 400 \text{ km s}^{-1}$ . We assumed  $300 \text{ km s}^{-1}$  since the distribution for  $\text{FWHM}([\text{O III}])$  for their entire type 2 sample falls off sharply at  $< 300 \text{ km s}^{-1}$ . In the end, this limit made little difference to the type 2 identification statistics.

Probable starburst/late-type starforming galaxies were classified using the negation of these single line ratios with some buffer to allow for flux errors, i.e., with:  $\log([\text{O III}]/\text{H}\beta) < 0.2$  or  $\log([\text{N II}]/\text{H}\alpha) < -0.3$  or  $\log([\text{S II}]/\text{H}\alpha) < -0.4$  or  $\log([\text{O III}]/[\text{O II}]) < -0.2$ .

EDITOR: PLACE TABLE 2 HERE.

It’s important to note that the type-2 AGN identified using the above single line pairs could be contaminated by low-metallicity emission-line galaxies or liners, especially at low redshift. Furthermore, the non-spectrophotometric nature of our spectra could invalidate some identifications made using widely separated lines (e.g., the pair  $[\text{O III}]$ ,  $[\text{O II}]$ ). These classifications are therefore very tentative given the quality of our data. We therefore declare all type 2 AGN identifications quoted in this paper to be probable. Follow-up with higher  $S/N$  spectral observations, preferably with better calibrated throughput as a function of wavelength will be needed for confirmation.



Early type galaxies were identified through the characteristic 4000 Å break, a signature caused by the dearth of hot and young (usually O and B-type) stars and strong heavy metal absorption by stellar photospheres. Stars were isolated by first ensuring that their radial velocities were  $\lesssim 150 \text{ km s}^{-1}$ . Their spectra were then matched to templates from the ELODIE stellar library (Moultaka et al. 2004). The majority were K and M dwarf stars. All other galaxy-like spectra with  $\text{H}\alpha$  or  $\text{H}\beta$   $\text{EW} > 5\text{\AA}$  but not fitting the above criteria, e.g., with single line measurements, or composites lying within  $1\text{-}\sigma$  ( $\pm 0.2$  dex) of the type 2/starburst classification boundaries in Figures 5 or 6 were classified as “unknown galaxies”.

## 4.2. Results Summary

Table 2 summarizes our source classifications. We only include our secure identifications for the type 1 AGN with probable identifications (as described in Section 3) placed in the “Unknown Galaxies” class. Also included are statistics for type 1 and type 2 AGN from the Cutri et al. (2002) northern 2MASS AGN survey, and the Francis et al. (2004) southern 2MASS AGN survey. The latter is broken into two color cuts. The Cutri et al. (2002) study has at least twice the detection rate for type 1 AGN. This could be due to deeper spectroscopic follow-up of fainter single targets in their study. It is possible that a significant fraction of our fainter targets at  $K_s > 14.5$  (e.g., Figure 1) where a spectral identification could not be secured are type 1 AGN. It’s also interesting to note that there is a tendency of the type 1 AGN identification rate to increase with  $J - K_s$  color in Table 2.

Figure 7 shows a sampling of spectra for the new type 1 AGN, primarily those with the highest redshifts. Two of the sources are at  $z > 1$ : 2MASS J21571362-4201497 with  $z = 1.321$  and 2MASS J10012986-0338334 with  $z = 1.389$ . The latter has been classified as a probable type 1 AGN due to a low spectral  $S/N$ , although given its relatively high redshift, it is most likely a QSO.

Table 3 lists the secure (T1) and probable (PT1) type 1 AGN identifications. There are 116 classified as T1 and 20 as PT1. Previous or alternative names as listed in the NASA Extragalactic Database (NED) are given. Of the 136 type 1 AGN, 8 (or  $\sim 6\%$ ) were previously classified as either “AGN”, “QSO” or “AGN/QSO?” in NED. Four of these are in the SDSS QSO sample. This implies a majority are new, previously undiscovered AGN. Interestingly, 10 of our type 1 AGN were previously detected in X-rays by the *ROSAT* All-Sky Survey (RASS). Table 4 lists the type 2 AGN, all of which are classified as probable using the methods described in Section 3. None of the type 2s were previously classified as AGN-like, and only one was detected in X-rays by the RASS. Of the previous classifications available in NED, a majority of our type 1 and 2 AGN are listed as galaxy-like and extended in the optical (SuperCOSMOS digitized plates) or near-IR (2MASS Atlas Images). At least 30% are also in the 2MASS Extended Source Catalog (XSC; Jarrett et al. 2000). This is expected given the depth of our sample.

EDITOR: PLACE FIGURE 7 HERE.

EDITOR: PLACE TABLE 3 HERE.

EDITOR: PLACE TABLE 4 HERE.

EDITOR: PLACE FIGURE 8 HERE.

## 5. Discussion

This section reviews the properties of our 2MASS AGN and compares them to those of AGN/QSOs discovered in optical surveys. We explore their redshift, luminosity, photometric and line equivalent-width distributions. Our primary benchmark and comparison sample of optically-selected AGN/QSOs is the SDSS Quasar Catalog Data Release 5 (DR5; Schneider et al. 2007). This catalog contains 2MASS matches to 9824 AGN, all within 2 arcsec.

### 5.1. Redshift and Luminosity Distributions

Our 2MASS AGN span the range  $0.01 \lesssim z \lesssim 1.38$  as shown in Figure 8 (*left*). The median  $z$  is  $\simeq 0.27$  and  $\simeq 0.21$  for type 1 and type 2 AGN respectively. A majority of our AGN are at low redshifts, with only two at  $z > 0.7$ . There are six securely identified AGN (4 type 1’s, 2 type 2’s) at  $z < 0.05$ . This is 24% (6/25) of all secure *galaxy*-like spectral identifications (including unknown types) in this redshift range. This is a lower limit since some objects classified as “unknown” could be type 2 AGN. Even removing our “probable” type 2 AGN, the AGN fraction is still relatively high. For comparison, Hao & Strauss (2004) find that  $\approx 4\%$  of  $\simeq 15,200$  SDSS-detected galaxies at  $z < 0.05$  harbor AGN (mostly Seyferts). An earlier study by Huchra & Burg (1992) found AGN (including LINERs) in  $\simeq 3.4\%$  of a sample of 2399 nearby blue-selected galaxies. These studies are not a fair comparison since the galaxies were optically selected. It would be of interest to determine the fraction of SDSS galaxies with active nuclei for a color cut of  $J - K_s > 2$ .

We have a significantly higher AGN identification rate than any previous low redshift galaxy sample. This is expected to be due to our red  $J - K_s$  color selection. The Francis et al. (2004) survey of 2MASS AGN had a bluer color cut,  $J - K_s > 1.2$ , and

had a significantly lower AGN fraction (see Section 4.2 and Table 2). Evidence for (low-luminosity) AGN activity was recently found in 17% of a sample of 64 late-type spiral galaxies by Desroches & Ho (2009) using X-ray data from *Chandra*. Wilkes et al. (2002) and Kuraszkiwicz et al. (2009) also showed that the 2MASS red AGN are generally weak X-ray emitters, with the reddest  $J - K_s$  sources being the weakest. AGN down to low luminosities are therefore more common than previously thought.

Another consideration is that the 6dF fiber diameter corresponds to sampling physical scales of  $R > 12.3 \text{ kpc } h_{70}^{-1}$  at  $z \geq 0.1$ . This means the 6dF spectra are sampling light from entire galaxies, even at the lowest redshifts. Furthermore, we are only sensitive to AGN with  $\text{H}\alpha$  or  $\text{H}\beta$   $\text{EW} > 5\text{\AA}$ . Ho et al. (1997) showed that we are likely to miss many AGN at this EW limit within our large aperture. From spectral observations of the nuclear regions ( $\lesssim 200 \text{ pc}$ ) of a large sample of blue-selected nearby galaxies, they found that almost 50% contain active nuclei. Even though galaxy light can significantly dilute the contribution from an AGN, we find that a near-IR selected sample with a red color cut can reduce the fraction of objects whose SEDs are dominated by host galaxy light, contrary to the claim of Ho et al. (1997).

Our redshift distribution is consistent with that from Cutri et al. (2002) who used a similar  $J - K_s$  color cut. They detected 2 QSOs with  $z > 2.3$ , consistent with an enhancement of the  $K_s$  band flux from  $\text{H}\alpha$  emission moving into that band. Figure 8 (right) shows  $J - K_s$  versus redshift for our AGN and SDSS QSOs. This shows that our red near-IR color criterion biases AGN selection towards low-redshifts because of the  $k$ -correction effect of the AGN/QSO SED. Most AGN show a sharp rise in flux in the rest-frame between 1 and  $2\mu\text{m}$ , possibly from hot dust emission (e.g., Sanders et al. 1989), and this is redshifted out of the  $K_s$  band at  $z \gtrsim 0.5$ . The  $J - K_s$  colors of SDSS QSOs and the prediction for radio-quiet QSOs from the template of Elvis et al. (1994) confirm this

trend. Barkhouse & Hall (2001) showed that 2MASS has the sensitivity to detect QSOs with  $J - K_s > 1.5$  out to  $z \simeq 4$ , maybe higher (see their Fig. 5), although they are very rare.

Figure 9 compares the  $K_s$  flux and luminosity between active and inactive galaxies as a function of redshift. We assumed a power-law SED  $f_\nu \propto \nu^{-\alpha}$  for the  $k$ -correction. The slope  $\alpha$  was derived from the  $J - K_s$  color of each source. No foreground reddening correction was applied since the extinction is typically  $A_K < 0.05$  mag for galactic latitudes  $|b| > 30^\circ$  (Schlegel et al. 1998).

Figure 9 (right) shows that the near-infrared luminosities of some of our active galaxies are comparable to those of securely identified inactive galaxies. These are a mixture of early-type and late-type starburst galaxies and their near-IR emission is dominated by the less-luminous host galaxy. Our AGN have a tail extending to higher luminosities (by  $\simeq 2$  mag) than the inactive galaxies. This trend has been found by many authors at other wavelengths (e.g., Huchra & Burg 1992; Hao & Strauss 2004). Also, host galaxy emission could be non-negligible in the type 2 AGN, suggesting they would be slightly less-luminous than the type 1s. This luminosity dependence is consistent with the observation that the fraction of type 1 AGN in our sample increases with redshift relative to inactive galaxies and there is a dearth of type 2 AGN at  $z > 0.4$ . For comparison, the bulk of the type 1 AGN extend to  $z \simeq 0.6$ .

EDITOR: PLACE FIGURE 9 HERE.

The  $K_s$  luminosities of our 2MASS AGN generally overlap with those of SDSS QSOs in the same redshift range, but the bulk at  $z > 0.2$  are more luminous on average than the locus formed by the SDSS QSOs (Figure 9 - *right*). Our AGN therefore have luminosities closer to QSOs than Seyferts, although we caution that the SDSS QSOs and 2MASS

AGN were selected using entirely different techniques. Figure 9 (*left*) shows that our AGN have a  $K_s$  flux limit ( $K_s = 15.5$ ) brighter by  $\gtrsim 0.5$  mag than the bulk of SDSS QSOs at similar redshifts. A large fraction of the SDSS QSOs at  $z \gtrsim 0.2$  are detected to fainter  $K_s$  magnitudes. The lower number of 2MASS AGN at  $K_s > 15$  is due to the higher incompleteness in spectral identifications at the faintest magnitudes. We are therefore sensitive to the most near-IR luminous objects of the optically selected QSO population.

The ratio of type 1 to type 2 AGN in our sample is  $\simeq 2 : 1$ . This ratio cannot be compared to studies at other wavelengths due to the high level of incompleteness in our sample, e.g., brought about by the relatively bright optical cut imposed by spectroscopy (see Section 3). However, compared to previous 2MASS AGN studies that performed follow-up spectroscopy to similar optical limits, there is tentative evidence that the type 1 to type 2 ratio depends on  $J - K_s$  color in the sense that a redder color cut has a higher proportion of type 1s. For example, Francis et al. (2004) find ratios of 14:23 and 4:0 for  $J - K_s > 1.2$  and  $> 1.8$  respectively, and Cutri et al. (2002) found  $\simeq 4 : 1$  for  $J - K_s > 2$  (Table 2). We find  $\simeq 2 : 1$  for an effective  $J - K_s \gtrsim 1.7$ . All these studies follow the same qualitative trend and cannot be explained by redshift or luminosity dependent biases. This is consistent with the notion that most type 2 AGN (e.g., Seyferts 2s) have their optical-to-near-IR emission dominated by “blue” host galaxy light, and that a red  $J - K_s$  cut will select more sources where the active nuclear emission dominates, i.e., type 1 AGN and QSOs at moderately low redshift.

EDITOR: PLACE FIGURE 10 HERE.

## 5.2. Broadband SEDs and Dust Reddening

Figure 10 compares the optical-to-near-IR colors of 2MASS red AGN to those of SDSS QSOs. The SDSS optical magnitudes were converted to equivalent UKST photographic  $b_J$ ,  $r_F$  magnitudes by first converting them to Cousins  $B$ ,  $V$  using the color corrections in Fukugita et al. (1995), and then to UKST magnitudes (on the Vega system) using the corrections in Blair & Gilmore (1982). Overall, the type 1 AGN span a range in  $b_J - K_s$  and  $b_J - r_F$  color similar to those of optically-selected SDSS QSOs at the same  $J - K_s$  color cut. This is not surprising since our sample required a relatively bright optical magnitude cut for reliable follow-up spectroscopy (see Section 2). We could indeed be sampling the same AGN population detected in the optical and spanning the same (low) redshift range (Figure 8 - *right*). Interestingly, the spread in  $b_J - K_s$  and  $b_J - r_F$  of the 2MASS red AGN are also consistent with the radio-loud quasar selected samples of Webster et al. (1995) and Francis et al. (2000), although these samples spanned a large range in redshift and very few sources were detected in all 2MASS bands.

The type 2 AGN have redder optical colors than the bulk spanned by type 1s (Figure 10 - *right*) where  $\Delta(b_J - r_F) \simeq 1$  mag. This is consistent with the AGN unified model where our view to the nuclear region is completely obscured and red host galaxy light will dominate the continuum flux at all wavelengths. The starlight can be intrinsically red (e.g., evolved stars), reddened by dust, or both. The type 1 AGN have bluer optical colours, consistent with the SDSS QSOs. The optical properties of 2MASS red type 1 AGN are therefore not dramatically different from those in optically selected samples.

Our spectral observations are not sufficiently spectrophotometric to warrant use of emission line ratios to constrain the amount of dust reddening. However, the distribution of optical and near-IR colors does not exclude mild amounts of dust reddening. Figure 10 shows reddening vectors for dust with an optical depth  $\tau_\lambda \propto 1/\lambda$  applied to the colors of a

typical blue QSO in the rest frame ( $z = 0$ ) and as observed at the median redshift of our type 1 AGN ( $z = 0.27$ ). In order for a “blue” QSO to be promoted to the region of color space occupied by the 2MASS red type 1 AGN, we require extinctions of  $A_V < 2$  mag. Note that there is evidence that the color-color locus occupied by the SDSS QSOs may already be extended by dust reddening with  $A_V \lesssim 1.5$  mag (Richards et al. 2003). This is to be compared to QSOs discovered in earlier optical/UV surveys that used more rigid selection criteria. For example, the LBQS (Hewett et al. 1995) spans  $0.6 \lesssim J - K_s \lesssim 1.4$ ,  $2 \lesssim b_J - K_s \lesssim 4$ , and  $0.5 \lesssim b_J - r_F \lesssim 1.5$ , considerably bluer than the SDSS QSOs. Using the LBQS as an unreddened comparison sample would make the 2MASS AGN colors more difficult to reconcile with a simple screen extinction model with  $\tau_\lambda \propto 1/\lambda$ . Most the 2MASS AGN are too blue in their optical colors for dust to be wholly responsible for modifying their optical/near-IR continua relative to blue-selected QSOs.

However, there is some evidence that at least some 2MASS AGN are reddened by dust. The SEDs for a sample of 10 very red 2MASS AGN with  $J - K_s > 2$ ,  $R - K_s > 5$  ( $b_J - K_s \gtrsim 5.5$ ) were modeled by Georgakakis et al. (2009). They found that all sources were consistent with moderate amounts of dust reddening of  $A_V = 1.3 - 3.2$  mag. They also found that the mid-IR SEDs are dominated by hot dust and that their  $60/12\mu\text{m}$  luminosity ratios are significantly higher than those of blue-selected Palomar-Green (PG) QSOs (Schmidt & Green 1983), suggesting a higher level of star-formation. Similar conclusions were reached by Kuraszkiewicz et al. (2009), including evidence that in a handful of highly polarized objects, the optical has a contribution from AGN light scattered by dust.

EDITOR: PLACE FIGURE 11 HERE.

We repeated a similar analysis as in Georgakakis et al. (2009) to determine whether our 2MASS red AGN have a significantly higher far-IR emission on average. A search



through the *Spitzer* and *ISO* archives turned up no mid-to-far IR data. However, eight type 1 AGN were securely detected by *IRAS* in all bands (12, 25, 60, and  $100\mu\text{m}$ ). One of these (2MASS J04225656-1854422) was previously identified as a Serfert 1 galaxy, another with an Ultra-Luminous IR Galaxy that was also detected in the RASS (2MASS J02460800-1132367), and the remainder are given a “Galaxy” classification in NED. The eight *IRAS* all-band-detected AGN span redshifts  $0.06 \leq z \leq 0.27$  and are at the red end of the  $b_J - K_s$  color distribution with  $b_J - K_s \gtrsim 4.5$ . Photometry was extracted from the *IRAS* Faint Source Catalog V2.0 using the IPAC Infrared Science Archive. In fact, only 10% of our 2MASS AGN (both type 1 and 2) were detected in at least one band by *IRAS*, indicating the 2MASS red AGN are not predominately associated with the ultraluminous IR QSOs found by Low et al. (1988).

Figure 11 shows the *rest-frame* optical-to-far-IR broad-band SEDs (at  $b_J$ ,  $r_F$ ,  $J$ ,  $H$ ,  $K_s$ , 12, 25, 60,  $100\mu\text{m}$ ) of this subsample of 2MASS AGN. The SEDs are normalized to the rest-frame  $12\mu\text{m}$  flux density since this wavelength is expected to be a relatively unbiased indicator of AGN power (e.g., Spinoglio & Malkan 1989), i.e., independent of dust extinction and star formation rate. The rest-frame  $12\mu\text{m}$  flux density was estimated by linearly interpolating between the  $12/(1+z)$  and  $25/(1+z)$  wavelengths in the rest frame. Figure 11 also shows the spread ( $25^{\text{th}}$  -  $75^{\text{th}}$  percentile range) observed for optically selected PG QSOs. These lines are directly from Georgakakis et al. (2009). The 2MASS red AGN all have higher normalized rest-frame far-IR emission at  $\lambda \gtrsim 80\mu\text{m}$  than the PG QSOs (at  $> 95\%$  significance). Three 2MASS AGN also have higher emission at rest-frame wavelengths  $50\mu\text{m} < \lambda < 60\mu\text{m}$ . This indicates the far-IR emission in at least a handful of 2MASS AGN is dominated by heated dust, either due to star formation, the central AGN or both. This same dust could contribute to reddenning of their optical-to-near-IR continua. It’s important to note that the 2MASS AGN with far-IR measurements are at the tail of distribution, i.e., just those with *IRAS* detections, and their IR SEDs are not necessarily

representative of 2MASS AGN in general.

### 5.3. Equivalent Width Distributions

Figure 12 shows  $b_J - K_s$  color as a function of equivalent width of the broad (permitted) emission line,  $H\beta$ , and the narrow (forbidden) emission line,  $[O\ III]$  ( $\lambda\ 5008\text{\AA}$ ). Traditionally, the broad emission lines are thought to originate from photoionized gas close to the central AGN known as the broad line region (BLR), and the narrow lines from much further out, to a few hundred parsecs or more, known as the narrow line region (NLR).

Overall, the  $H\beta$  and  $[O\ III]$  EW distributions for our type 1 AGN are consistent with those of optically selected quasars (e.g., from SDSS). However, there is a clear separation in these EWs between our type 1 and 2 AGN and this is consistent with the AGN unified model. The  $H\beta$  line in most of the type 2 AGN appears intrinsically weaker than that in type 1s. This is because fewer ionizing photons are reaching and being reprocessed by the NLR, e.g., due to absorption and scattering by dust. In type 1s, we have a direct view of the BLR line emission. Emission from the NLR can also contribute to the observed  $H\beta$  line flux in type 1s. The type 2 AGN also appear to be redder on average in  $b_J - K_s$  than the type 1s. This is also consistent with the unified model if the continuum flux in type 2s suffers more extinction from dust, or if obscuration of the central AGN allows us to see more contribution from a “redder” host galaxy, e.g., from old stellar populations.

EDITOR: PLACE FIGURE 12 HERE.

The behavior in the EW of the narrow  $[O\ III]$  emission line (Figure 12 - *right*) for type 1 and 2 AGN is reversed. Here, the  $[O\ III]$  emission from type 1s is reduced relative to the optical continuum because the latter is stronger (e.g., less extinguished by dust) than

that in type 2s. This is consistent with the difference in  $b_J - K_s$  color between the type 1 and 2 AGN being due to dust reddening. Interestingly,  $b_J - K_s$  color is weakly but significantly correlated with [O III] EW for each of the type 1 and type 2 classes. Pearson’s product-moment correlation coefficient is 0.29 and 0.32 for the type 1s and type 2s respectively, with probabilities of  $<0.1\%$  and  $<0.8\%$  of these measures occurring by chance. Similar results are obtained using Kendall’s non-parametric  $\tau$  test.

These results suggest anisotropic obscuration of the central AGN and BLR, and the bulk of the narrow-line emission originates from beyond the obscuring material. The type 2 AGN in particular require contamination by non-AGN light (e.g., galaxy hosts) if the AGN continuum source is obscured. Otherwise their [O III] EWs will be much larger than observed. Scattered AGN light cannot account for the additional continuum since it is expected to be less than a few percent in these objects (Kuraszkiewicz et al. 2009). Also, the overlap in EWs between our type 1 AGN and optically selected QSOs implies host-galaxy contamination to their optical continuum emission is minimal.

## 6. Conclusions

We have extended the 2MASS red AGN search to the southern equatorial sky and increased the statistical base of red AGN by  $\simeq 35\%$  relative to previous surveys (primarily from Cutri et al. 2002). We used the unique capabilities of the 6dF instrument and efficient observing strategy of the 6dF Galaxy Redshift Survey to acquire spectra for 1182 candidates selected from the 2MASS PSC. Our main conclusions are

1. Classifications were secured for 432 spectra, of which 116 were securely identified as type 1 AGN with broad permitted emission lines exceeding  $1000 \text{ km s}^{-1}$  (FWHM). 57 were identified as type 2 AGN, all of which are tentative due to the non-

spectrophotometric nature of their spectra, availability of appropriate emission line pairs, and line flux measurement uncertainties.

2. A majority of the type 1 AGN are new, with only eight (or  $\sim 6\%$ ) previously identified as AGN or QSOs in the literature. Most of them were previously classified as galaxy-like and extended in the optical (SuperCOSMOS digitized plates) or near-IR (2MASS Atlas Images). 95% span the redshift range  $0.05 < z < 0.5$ .
3. Our selection method finds a significantly higher fraction of local galaxies containing AGN than in previous blue-selected galaxy surveys. Our red ( $J - K_s \gtrsim 2$ ) color cut selects against intrinsically blue galaxy light. We find that  $\simeq 24\%$  of our objects at  $z < 0.05$  are associated with an AGN. For comparison, blue-selected galaxy samples are finding  $\simeq 4\%$ .
4. Comparing our ratio of type 1 to type 2 AGN to that found in previous studies of 2MASS red AGN, there is tentative evidence that this ratio increases with a redder  $J - K_s$  color cut. This is consistent with the observation that most type 2 AGN have their optical-to-near-IR emission dominated by blue galaxy light, and that a redder  $J - K_s$  cut will select more sources where the active nuclear emission dominates, i.e., type 1 AGN.
5. The optical colors of the 2MASS AGN constrain any extinction by dust to be  $A_V < 2$  mag relative to the SEDs of blue optically-selected QSOs. Most of the type 1 AGN are too blue in their optical colors for dust to significantly affect their optical/near-IR continua. There are also a handful of red type 1 AGN (with  $b_J - K_s \gtrsim 4.5$ ) showing excess far-IR emission at  $\lambda \gtrsim 80\mu\text{m}$ , and some at  $50\mu\text{m} < \lambda < 60\mu\text{m}$ . This suggests at least some 2MASS AGN reside in dusty environments.

6. The distribution of  $H\beta$  and  $[O\ III]$  equivalent widths, and optical/near-IR colors for type 1 and 2 AGN are consistent with AGN unified models. The equivalent width of the  $[O\ III]$  emission line correlates with  $b_J - K_s$  color in both types of AGN, suggesting anisotropic obscuration of the central AGN. The type 2 AGN require a significant contribution to their optical continua by stellar light to satisfy the equivalent width measurements.
7. Overall, the optical properties of the 2MASS red AGN are not dramatically different from those found in optical QSO samples. This is most likely due to the relatively bright optical magnitude limit imposed for reliable spectroscopic identification. It appears that red AGN selection in 2MASS detects the most luminous objects in the near-IR in the local universe to  $z \simeq 0.6$ . This is impetus to use similar methods for future deep near-IR surveys. Indeed, such surveys have already begun to unravel a new population of AGN at high redshift.

This publication makes use of data products from the Two Micron All Sky Survey, which is a joint project of the University of Massachusetts and the Infrared Processing and Analysis Center/California Institute of Technology, funded by the National Aeronautics and Space Administration and the National Science Foundation. Funding for the SDSS and SDSS-II has been provided by the Alfred P. Sloan Foundation, the Participating Institutions, the National Science Foundation, the U.S. Department of Energy, the National Aeronautics and Space Administration, the Japanese Monbukagakusho, the Max Planck Society, and the Higher Education Funding Council for England. The SDSS Web Site is <http://www.sdss.org/>. This research has made use of the NASA/IPAC Extragalactic Database (NED) and the NASA/IPAC Infrared Science Archive (IRSA), which are operated by the Jet Propulsion Laboratory, California Institute of Technology, under contract with the National Aeronautics and Space Administration. The 6dFGS was carried out by the

Anglo-Australian Observatory and the 6dFGS team<sup>3</sup>, who have all contributed to the work presented here. This work was carried out at the California Institute of Technology, with funding from the National Aeronautics and Space Administration. RMC acknowledges support from the National Academy of Sciences James Craig Watson Medal award. JPH was supported in part by NSF Grant AST0406906. We thank the anonymous referee for helpful comments.

*Facilities:* CTIO:2MASS, UKST (6dF)

---

<sup>3</sup><http://www.aao.gov.au/local/www/6df/6dFGSteam.html>

## REFERENCES

- Baldwin, J. A., Phillips, M. M., & Terlevich, R., 1981, *PASP*, 93, 5
- Barkhouse, W. A. & Hall, P. B., 2001, *AJ*, 121, 2843
- Benn, C. R., Vigotti, M., Carballo, R., Gonzalez-Serrano, J. I., & Sánchez, S. F., 1998, *MNRAS*, 295, 451
- Blair, M., & Gilmore, G., 1982, *PASP*, 94, 742
- Brown, M. J. I., et al., 2006, *ApJ*, 638, 88
- Colless, M., et al., 2001, *MNRAS*, 328, 1039
- Croom, S. M., Warren, S. J., & Glazebrook, K., 2001, *MNRAS*, 328, 150
- Cutri, R. M., Nelson, B. O., Francis, P. J., & Smith, P. S., 2002, in *ASP Conference Proceedings*, Vol. 284, eds R. F. Green, E. Ye. Khachikian, and D. B. Sanders, p. 127
- Desroches, L.-B., & Ho, L., 2009, *ApJ*, 690, 267
- Donley, J. L., Rieke, G. H., Pérez-González, P. G., & Barro, G., 2008, *ApJ*, 687, 111
- Elvis, M., Wilkes, B. J., McDowell, J. C., Green, R. F., Bechtold, J., Willner, S. P., Oey, M. S., Polomski, E., & Cutri, R., 1994, *ApJS*, 95, 1
- Francis, P. J., Whiting, M. T., & Webster, R. L., 2000, *PASA*, 17, 56
- Francis, P. J., Nelson, B. O., & Cutri, R. M., 2004, *AJ*, 127, 646
- Fraquelli, H. A., & Storchi-Bergmann, T., 2004, *Proceedings of IAU Symposium 222*, eds T. Storchi-Bergmann, L.C. Ho, and Henrique R. Schmitt. Cambridge, UK: Cambridge University Press, p. 319

- Fukugita, M., Shimasaku, K., & Ichikawa, T., 1995, *PASP*, 107, 945
- Georgakakis, A., Clements, D. L., Bendo, G., Rowan-Robinson, M., Nandra, & K.,  
Brotherton, M. S., 2009, *MNRAS*, 394, 533
- Glikman, E., Gregg, M. D., Lacy, M., Helfand, D. J., Becker, R. H., & White, R. L., 2004,  
*ApJ*, 607, 60
- Glikman, E., Helfand, D. J., White, R. L., & Becker, R. H., 2007, *ApJ*, 667, 673
- Gregg, M. D., Lacy, M., White, R. L., Glikman, E., Helfand, D., Becker, R. H., &  
Brotherton, M. S., 2002, *ApJ*, 564, 133
- Hambly, N. C., et al., 2001a, *MNRAS*, 326, 1279
- Hambly, N. C., et al., 2001b, *MNRAS*, 326, 1295
- Hao, L., & Strauss, M. A., 2004, *Carnegie Observatories Astrophysics Series, Vol. 1.,  
Coevolution of Black Holes and Galaxies* (Cambridge: Cambridge University Press)
- Hewett, P. C., Foltz, C. B., & Chaffee, F. H., 1995, *AJ*, 109, 1498
- Ho, L. C., Filippenko, A. V., & Sargent, W. L. W., 1997, *ApJS*, 112, 315
- Ho, L. C., ed. 2004, *Carnegie Observatories Astrophysics Series, Vol. 1., Coevolution of  
Black Holes and Galaxies* (Cambridge: Cambridge University Press)
- Huber, P. J., 1981, *Wiley Series in Probability and Mathematical Statistics*, (New York:  
Wiley)
- Huchra, J., & Burg, R., 1992, *ApJ*, 393, 90
- Jarrett, T. H., Chester, T., Cutri, R., Schneider, S., Skrutskie, M., & Huchra, J. P., 2000,  
*AJ*, 119, 2498



- Jarrett, T. H., 2004, PASA, 21, 396
- Jones, D. H., et al., 2004, MNRAS, 355, 747
- Jones, D. H., et al., 2009, MNRAS, in press (arXiv:0903.5451)
- Jurek, R. J., Drinkwater, M. J., Francis, P. J., & Pimblet, K. A., 2008, MNRAS, 383, 673
- Kewley, L. J., Heisler, C. A., Dopita, M. A., & Lumsden, S., 2001, ApJS, 132, 37
- Kewley, L. J., Groves, B., Kauffmann, G., & Heckman, T., 2006, MNRAS, 372, 961
- Kuraszkiewicz, J., Wilkes, B. J., Schmidt, G., Ghosh, H., Smith, P. S., Cutri, R., Hines, D.,  
Huff, E. M., McDowell, J. C., & Nelson, B., 2009, ApJ, 692, 1143
- Low, F. J., Cutri, R. M., Huchra, J. P., & Kleinmann, S. G., 1988, ApJ, 327, L41
- Maddox, N., Hewett, P. C., Warren, S. J., & Croom, S. M., 2008, MNRAS, 386, 1605
- Masci, F. J., Webster, R. L., & Francis, P. J., 1998, MNRAS, 301, 975
- Moultaka, J., Ilovaisky, S. A., Prugniel, P., & Soubiran, C., 2004, PASP, 116, 693
- Polletta, M., et al., 2007, ApJ, 663, 81
- Richards, G. T., et al., 2002, AJ, 123, 2945
- Richards, G. T., et al., 2003, AJ, 126, 1131
- Sanders, D. B., Phinney, E. S., Neugebauer, G., Soifer, B. T., & Matthews, K., 1989, ApJ,  
347, 29
- Saunders, W., et al., 2001, Anglo-Australian Observatory Newsletter, 97, 14
- Schneider, D. P., 2007, et al., AJ, 134, 102

- Schlegel, D. J., Finkbeiner, D. P., & Davis, M., 1998, *ApJ*, 500, 525
- Schmidt, M., & Green, R. F., 1983, *ApJ*, 269, 352
- Sharp, R. G., Sabbey, C. N., Vivas, A. K., Oemler, A., McMahon, R. G., Hodgkin, S. T., & Coppi, P. S., 2002, *MNRAS*, 337, 1153
- Skrutskie, M. F., et al., 2006, *AJ*, 131, 1163
- Smail, I., Sharp, R., Swinbank, A. M., Akiyama, M., Ueda, Y., Foucaud, S., Almaini, O., & Croom, S., 2008, *MNRAS*, 389, 407
- Smith, P. S., Schmidt, G. D., Hines, D. C., Cutri, R. M., Nelson, B. O., 2002, *ApJ*, 569, 23
- Spinoglio, L., & Malkan, M. A., 1989, *ApJ*, 342, 83
- Vanden Berk, D. E., et al., 2001, *AJ*, 122, 549
- Veron-Cetty, M. P. & Veron, P., 2000, *ESO Sci. Rep.*, 19, 1
- Warren, S J., Hewett, P. C., & Foltz, C. B., 2000, *MNRAS*, 312, 827
- Watson, F. G., Parker, Q. A., Miziarski, S., 1998, *SPIE*, 3355, 834
- Webster, R. L., Francis, P. J., Peterson, B. A., Drinkwater, M. J., & Masci, F. J., 1995, *Nature*, 375, 469
- Wilkes, B. J., Schmidt, G. D., Cutri, R. M., Ghosh, H., Hines, D. C., Nelson, B., Smith, P. S., 2002, *ApJ*, 564, L65
- Zakamska, N. L., et al., 2003, *AJ*, 126, 2125

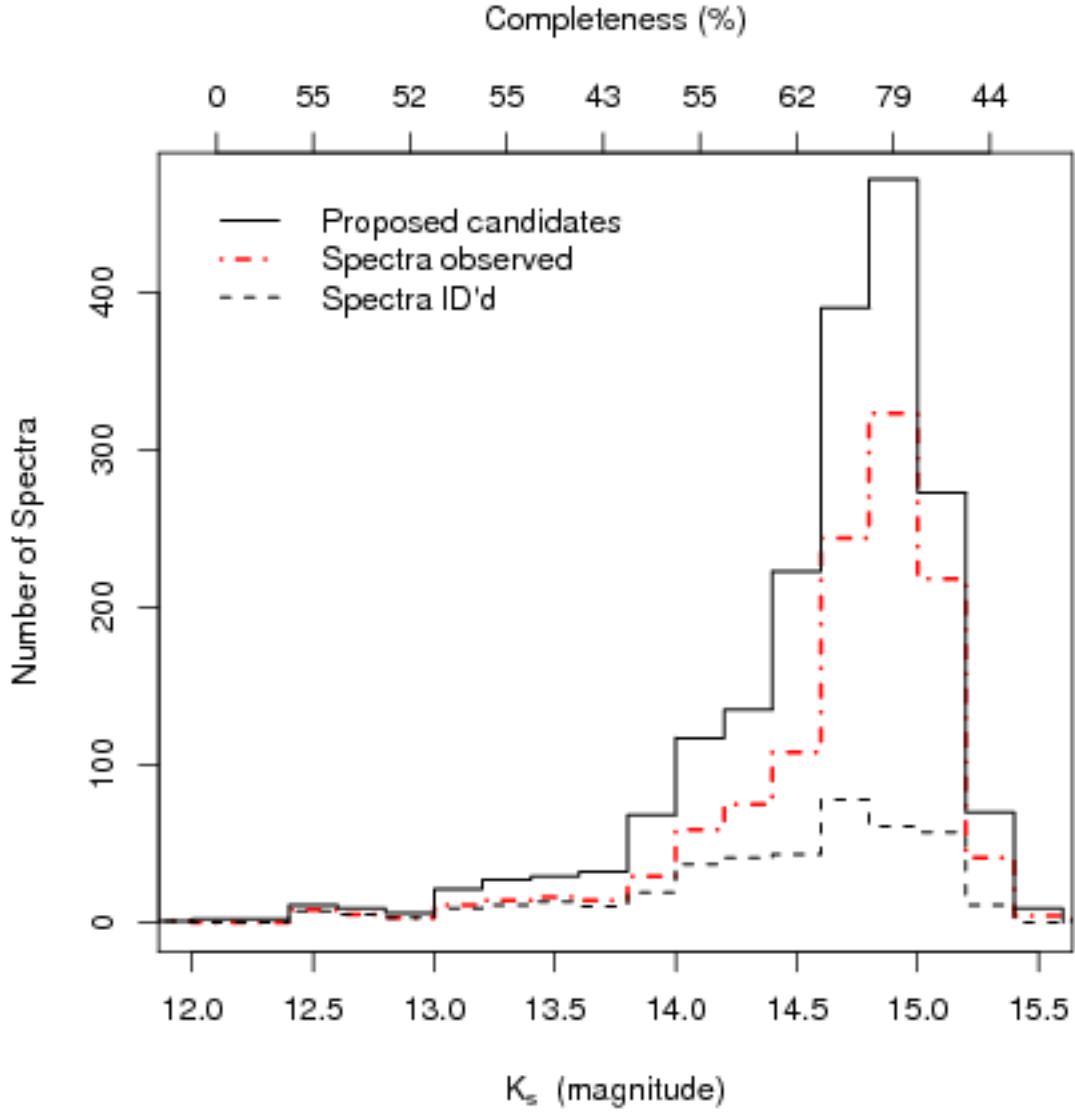


Fig. 1.—  $K_s$  brightness distribution of proposed AGN candidates, sources with observed spectra, and sources for which we secured a reliable spectral identification. The top horizontal axis shows the approximate completeness (= number spectra observed/number candidates) for several magnitude bins.

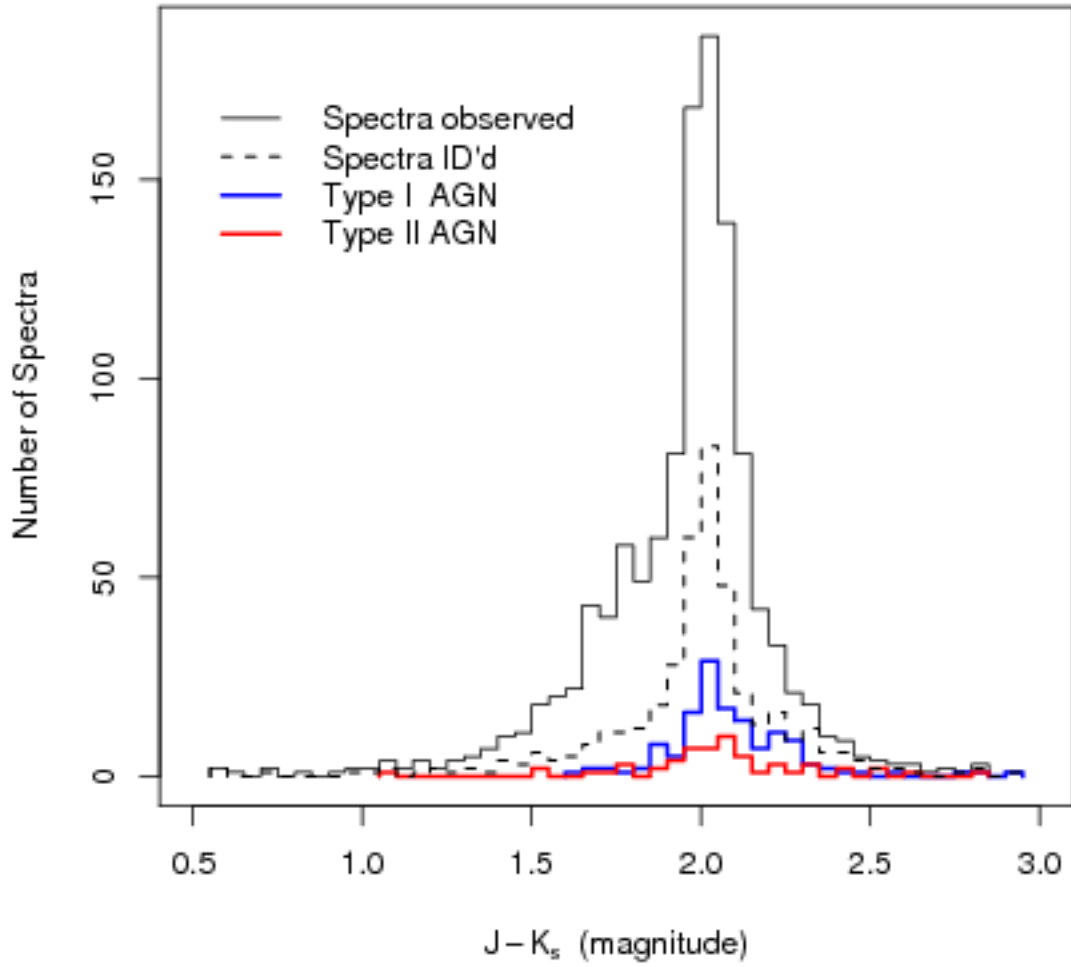


Fig. 2.—  $J - K_s$  color distribution of sources with observed spectra, sources for which we secured a reliable spectral identification, and those identified as Type-1 and Type-2 AGN.

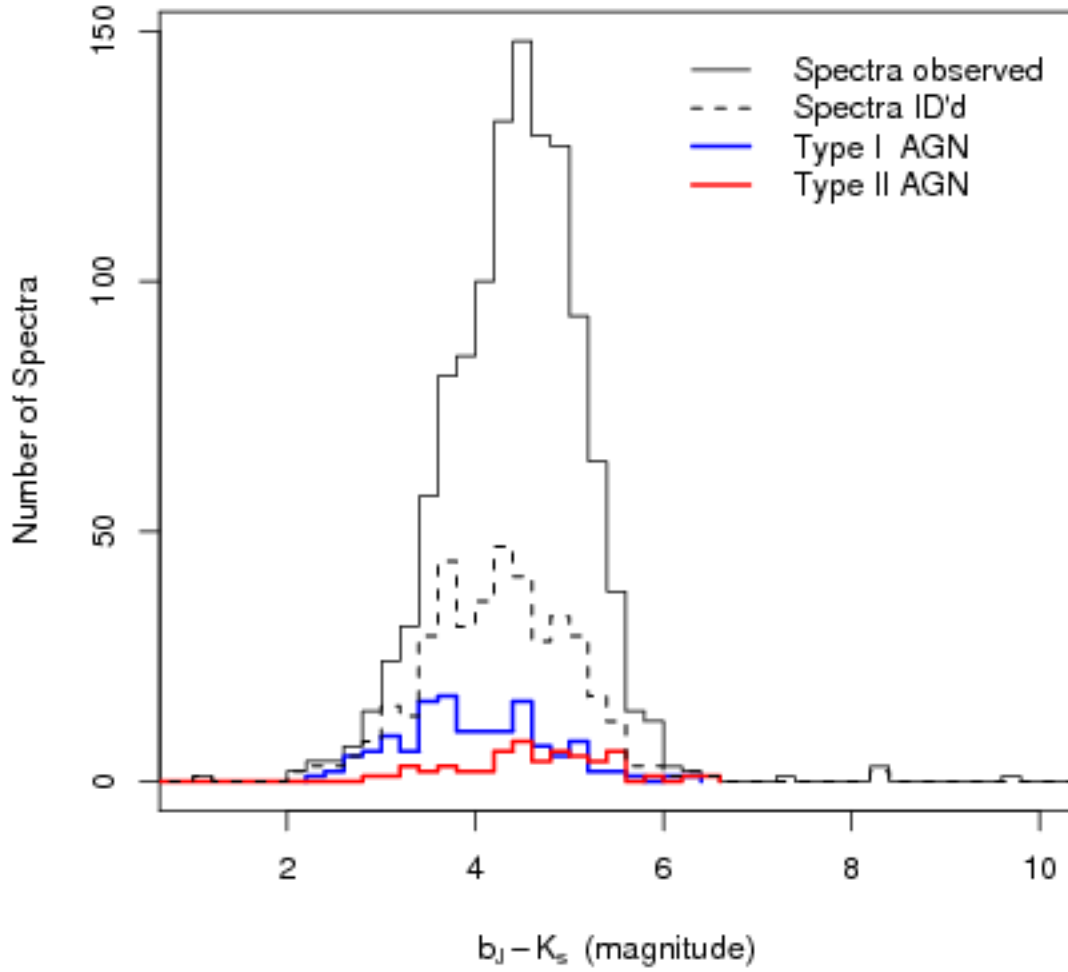


Fig. 3.—  $b_J - K_s$  color distribution of sources with observed spectra, sources for which we secured a reliable spectral identification, and those identified as Type-1 and Type-2 AGN.

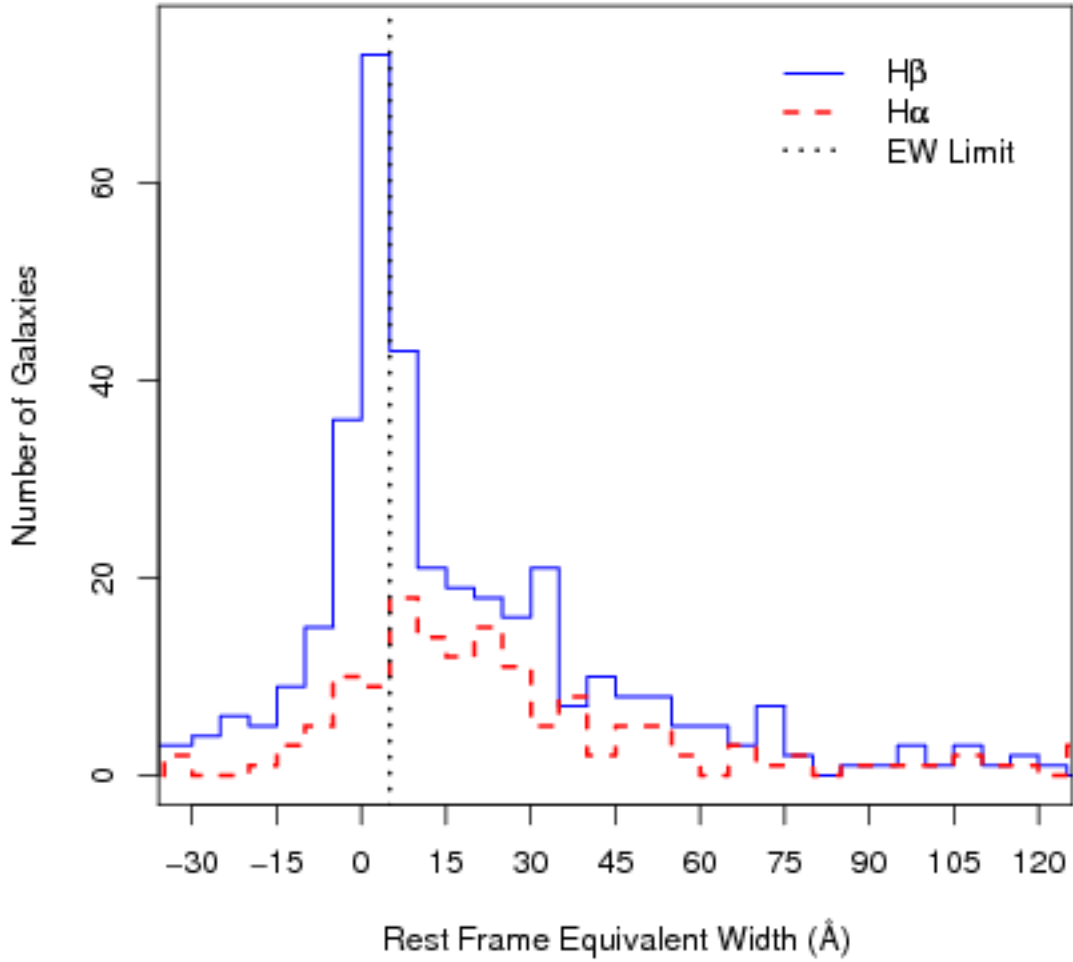


Fig. 4.— Distribution of rest-frame H $\alpha$  and H $\beta$  equivalent widths for all galaxies with the best quality spectra. We are sensitive to all equivalent widths to the right of the vertical dotted line ( $> 5\text{\AA}$ ).

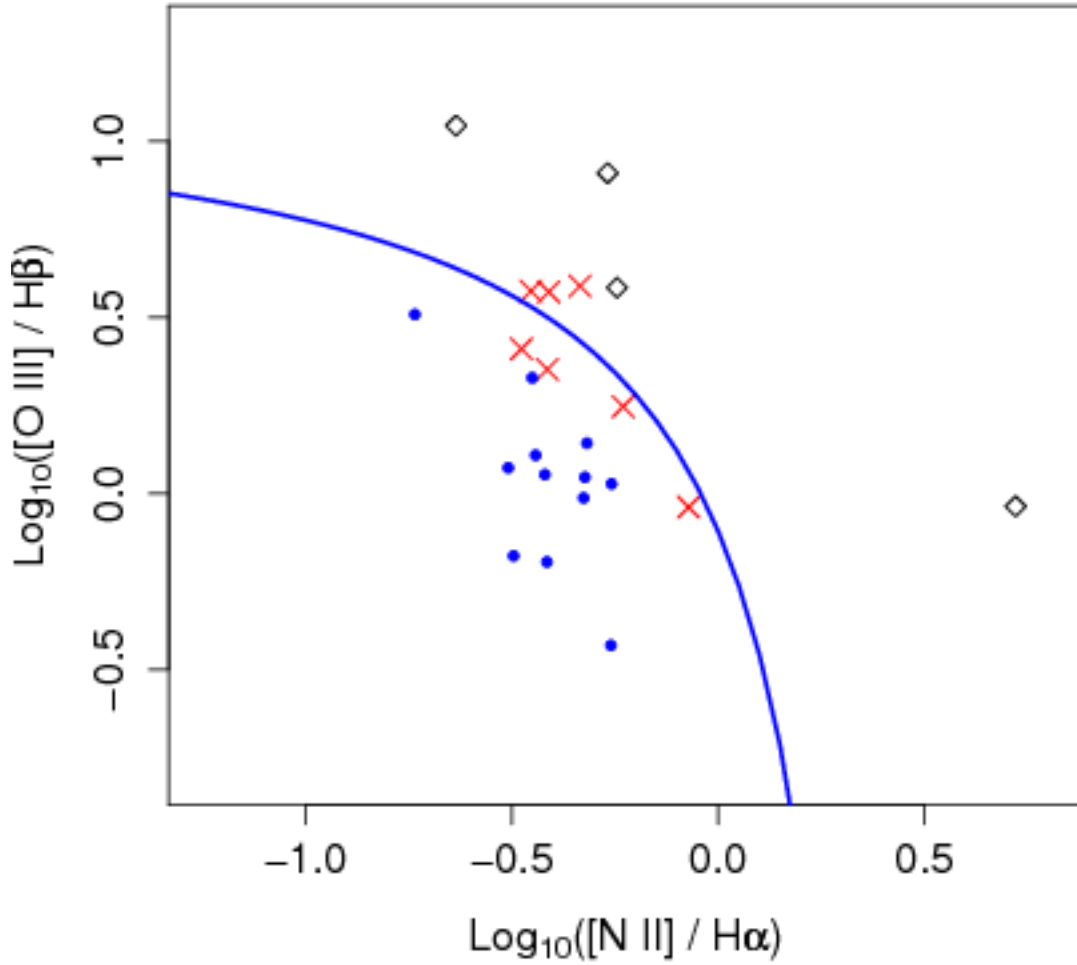


Fig. 5.— Line ratio diagram for galaxies with type 1 AGN classifications removed. Diamonds and filled circles are “probable” type 2 AGN and star-forming galaxies respectively, all at  $\geq 0.2$  dex ( $1-\sigma$ ) from the classification boundary of Kewley et al. (2001, solid line). Crosses are composites (classified as unknown galaxies). Errors in the line ratios are typically 0.2 dex ( $1-\sigma$ ).

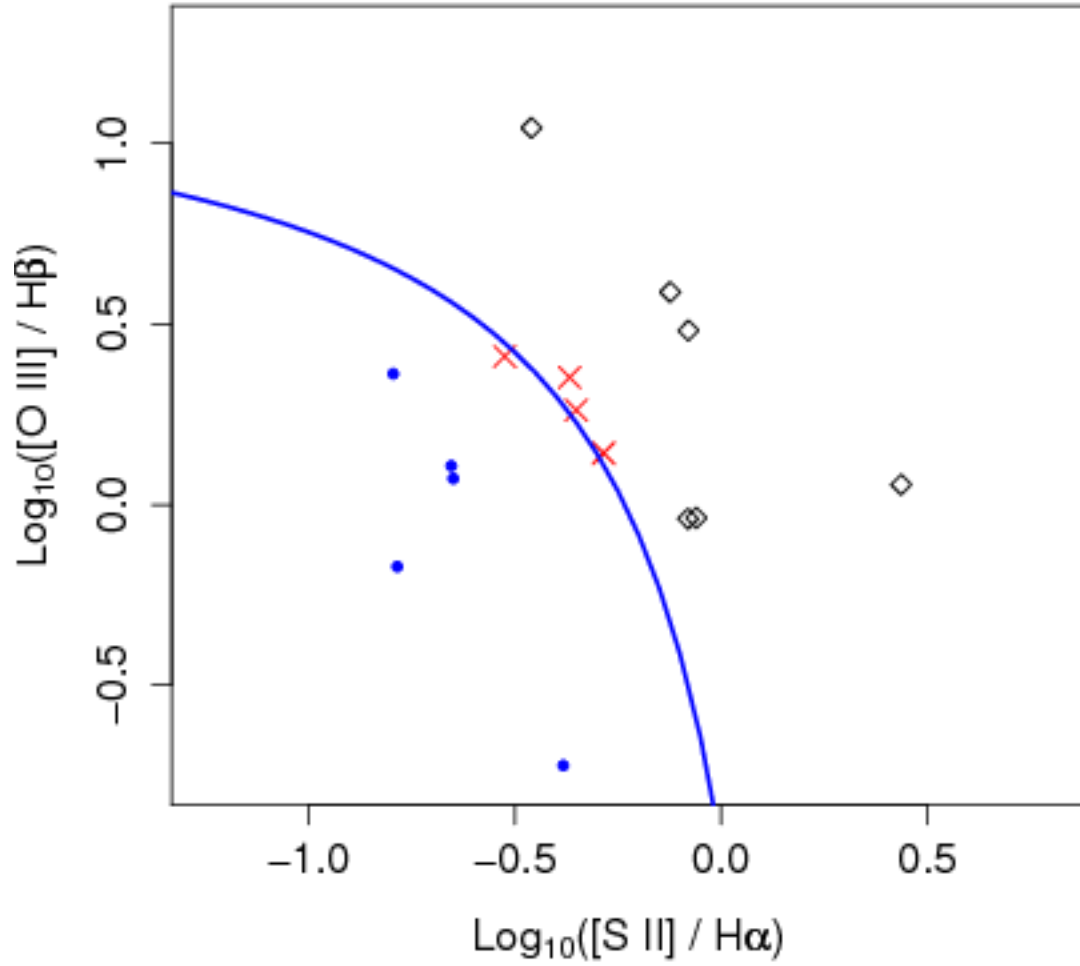


Fig. 6.— Same as Figure 5 but with  $[\text{S II}]$  in the abscissa. The solid line is the AGN/star-formation discriminator from Kewley et al. (2001). Errors in the line ratios are typically 0.2 dex ( $1-\sigma$ ).



**Figure 7 available at:**

**<http://web.ipac.caltech.edu/staff/fmasci/home/miscscience/f7.jpg>**

Fig. 7.— Rest frame spectra of some new type 1 AGN overlaid with emission lines typically found in QSO spectra. The spectra for all objects listed in Tables 3 and 4 can be viewed by querying the 6dF public database: <http://www.aao.gov.au/6dFGS/>.

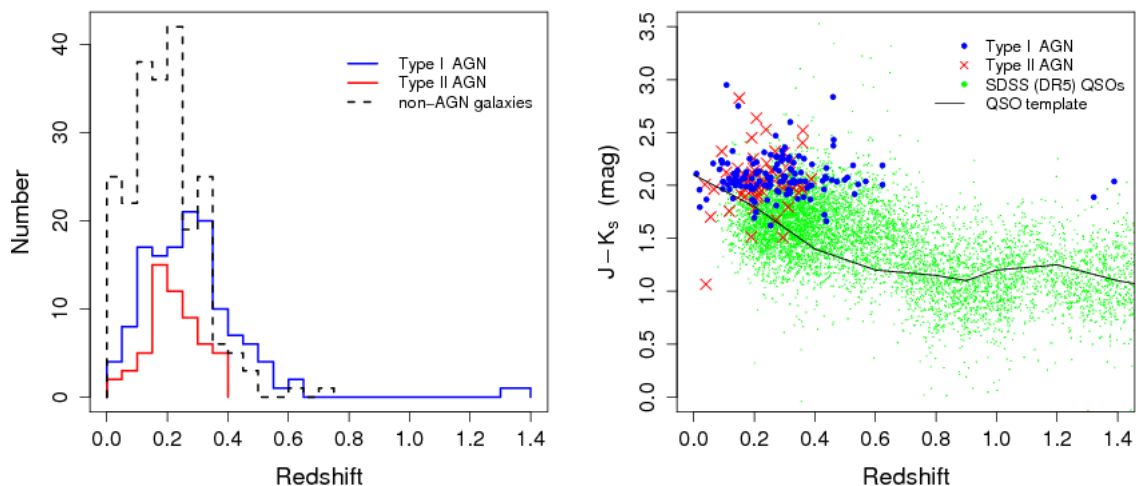


Fig. 8.— (*left*) Redshift distributions for our type 1 and 2 AGN, and inactive galaxies with good quality spectra including “unknown” galaxy types. (*right*)  $J - K_s$  color versus redshift for our type 1 and 2 AGN, and SDSS QSOs. The line shows the prediction for radio-quiet QSOs using the template of Elvis et al. (1994). Uncertainties in  $J - K_s$  are  $\lesssim 0.16$  mag ( $1-\sigma$ ).

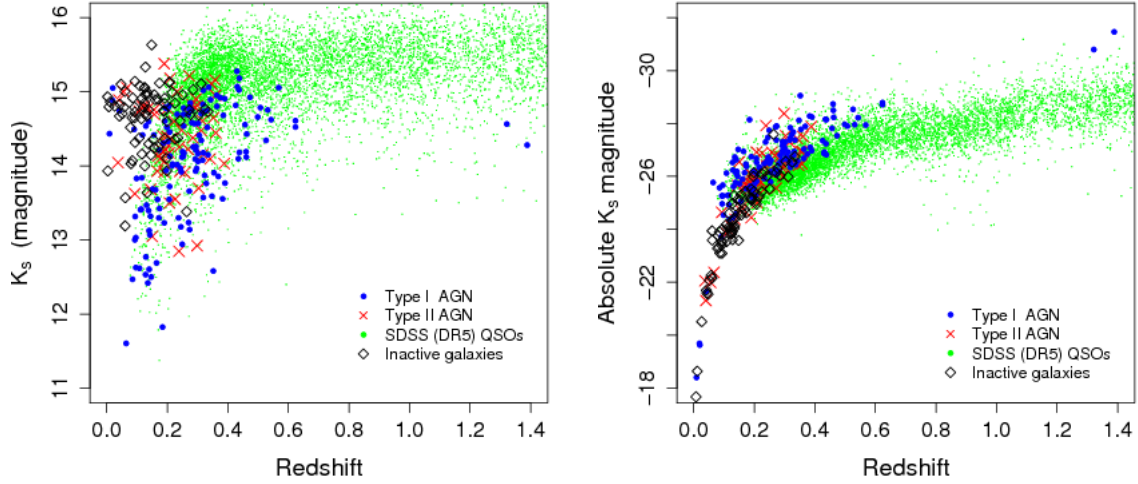


Fig. 9.— Apparent  $K_s$  magnitude (*left*) and absolute  $K_s$  magnitude (*right*) as a function of redshift for 2MASS AGN, SDSS QSOs, and *securely* identified inactive galaxies in our sample where “unknown” classifications were omitted.

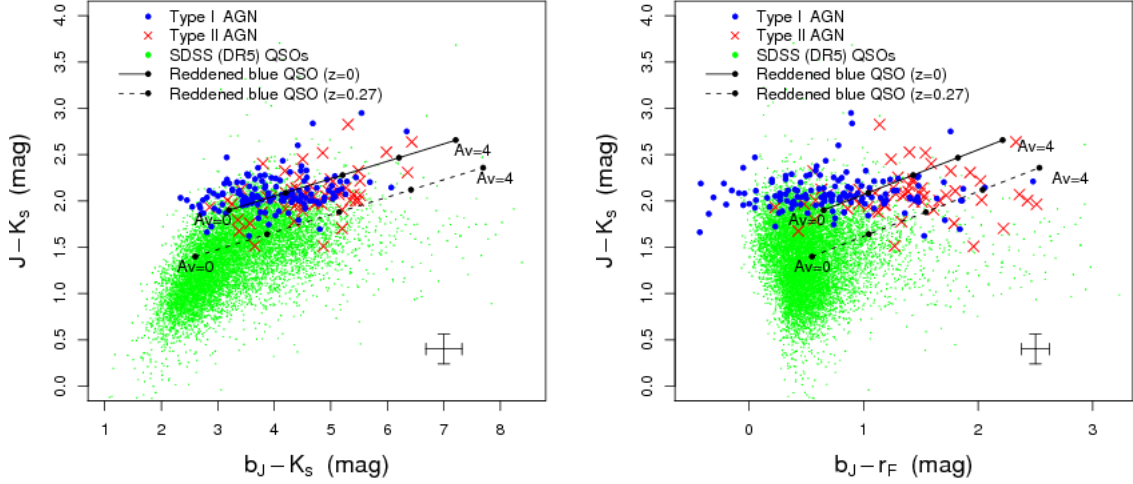


Fig. 10.— Color-color plots involving  $b_J$ ,  $r_F$ ,  $J$ ,  $K_s$  for 2MASS red AGN and SDSS QSOs. The lines with filled dots indicate changes in colors due to pure dust reddening of a fiducial blue QSO assuming a  $1/\lambda$  extinction law at  $z = 0$  (solid lines), and at the median redshift of our type 1 AGN,  $z = 0.27$  (dashed lines). These predictions assume the intrinsic (unreddened) colors of a QSO from the median composite of Elvis et al. (1994). The vertical/horizontal lines denote (maximum)  $1\text{-}\sigma$  uncertainties along each axis:  $\simeq 0.32$ ,  $0.12$ , and  $0.16$  mag for  $b_J - K_s$ ,  $b_J - r_F$ , and  $J - K_s$  respectively.

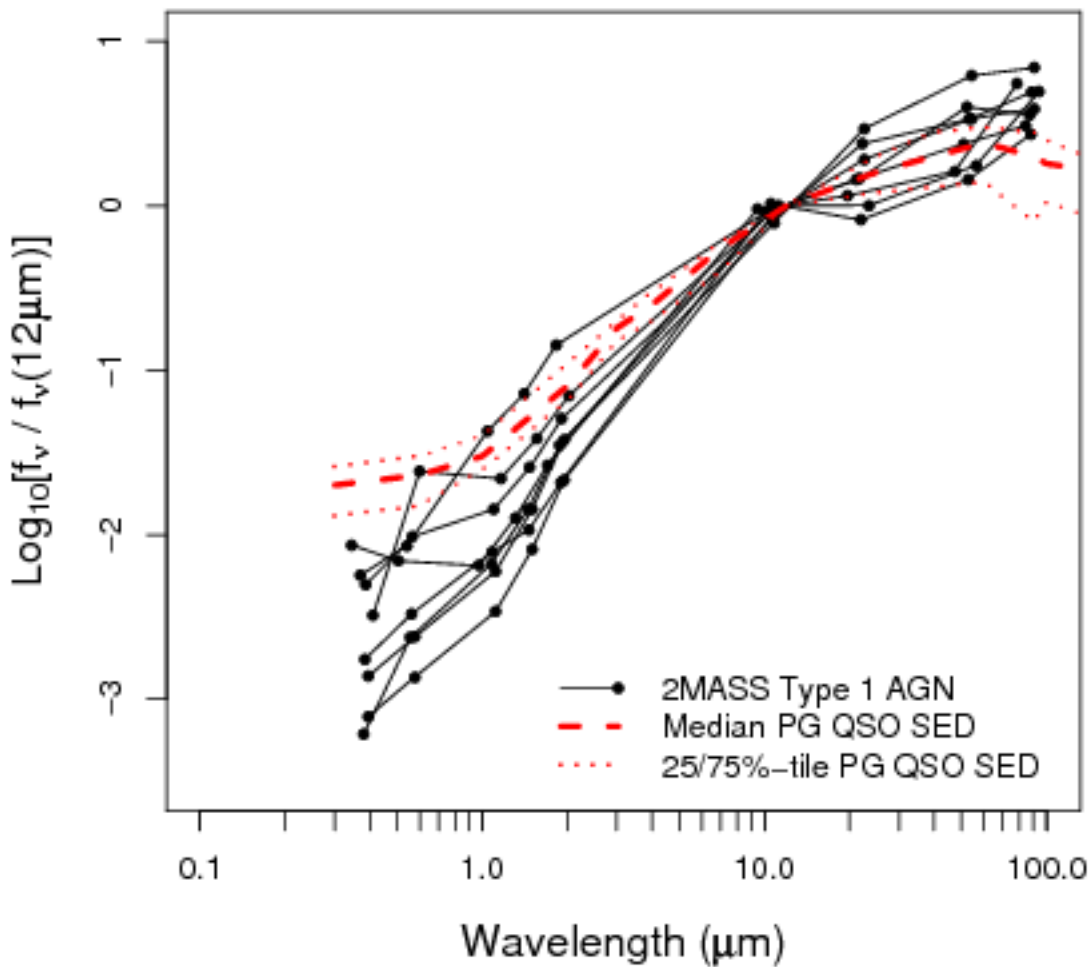


Fig. 11.— Rest-frame SEDs of *IRAS* detected 2MASS type 1 AGN (dots connected with lines) and the median, 25<sup>th</sup>, and 75<sup>th</sup> percentiles of PG QSO SEDs from Georgakakis et al. (2009, dashed and dotted lines). These authors used survival statistics to account for upper limits in the flux measurements of PG QSOs. All SEDs are normalized to a linearly interpolated rest-frame 12μm flux density (see text for details).

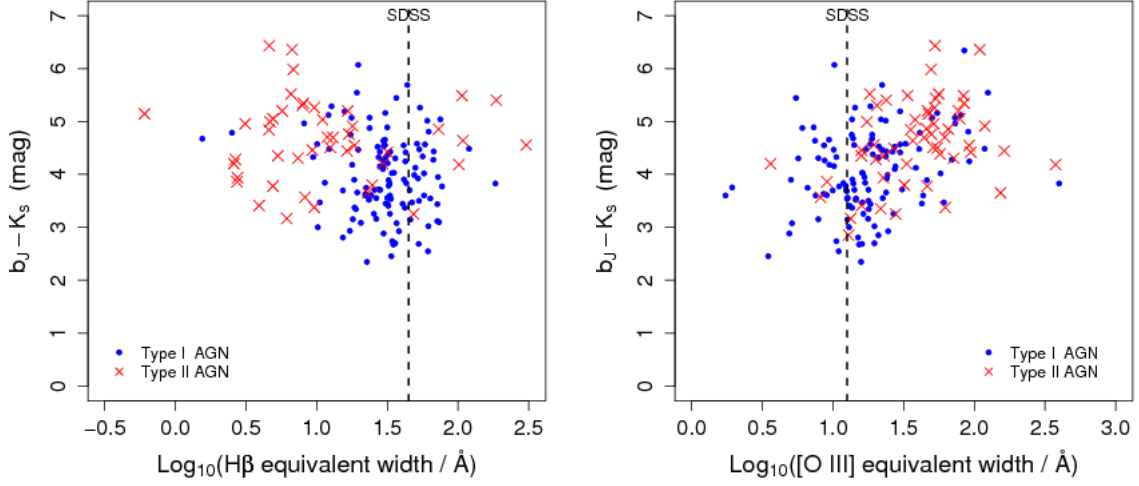


Fig. 12.—  $b_J - K_s$  color as a function of rest frame  $\text{H}\beta$  equivalent width (*left*) and rest frame  $[\text{O III}]$  equivalent width (*right*) for the 2MASS type 1 and 2 AGN. Dashed vertical lines show equivalent widths from the SDSS median composite spectrum of Vanden Berk et al. (2001).  $1-\sigma$  uncertainties are  $\lesssim 0.32$  mag in  $b_J - K_s$  and  $\lesssim 0.18$  in  $\text{log}_{10}(\text{EW})$ .

Table 1: Rest wavelength regions used in emission-line measurements.

| Line       | Center <sup>a</sup><br>(Å) | Continuum Integration Limits<br>(Å) | Line Integration Limits<br>(Å) |
|------------|----------------------------|-------------------------------------|--------------------------------|
| C III]     | 1908.73                    | 1800–1850, 1970–2010                | 1860–1955                      |
| Mg II      | 2798.75                    | 2650–2700, 3000–3050                | 2750–2850                      |
| [O II]     | 3728.48                    | 3650–3700, 3770–3815                | 3710–3740                      |
| H $\beta$  | 4862.68                    | 4740–4840, 4880–4940                | 4845–4880                      |
| [O III]    | 5008.24                    | 4880–4940, 5030–5100                | 4990–5025                      |
| H $\alpha$ | 6564.61                    | 6400–6520, 6630–6700                | 6550–6572                      |
| [N II]     | 6585.28                    | 6400–6520, 6630–6700                | 6572–6594                      |
| [Si II]    | 6725.48 <sup>b</sup>       | 6630–6700, 6745–6845                | 6700–6745                      |

<sup>a</sup>As defined in Vanden Berk et al. (2001)

<sup>b</sup>Average of doublet [Si II]  $\lambda\lambda$ 6718.29, 6732.67

Table 2. Source classifications and comparisons to previous studies.

|                           | This Study<br>( $J - K_s \gtrsim 1.7$ ) | Cutri et al. (2002)<br>( $J - K_s > 2.0$ ) | Francis et al. (2004)<br>( $J - K_s > 1.2$ ) | Francis et al. (2004)<br>( $J - K_s > 1.8$ ) |
|---------------------------|---|--|--|--|
| Number Classified         | 432                                     | 664  | 1304   | 66   |
| Stars (%)                 | 23 (5.3) <sup>a</sup>                   | 66 (9.9)                                   | 330 (25.3)                                   | 6 (9.1)                                      |
| Unknown Galaxies (%)      | 193 (44.7)                              | ...  | ...  | ...  |
| Early-type Galaxies (%)   | 17 (3.9)                                | ...  | ...  | ...  |
| SB/Late-type Galaxies (%) | 26 <sup>c</sup> (6.0)                   | ...  | 106 (8.1)                                    | ...  |
| Type 1 AGN (%)            | 116 <sup>b</sup> (26.8)                 | 385 (57.9)                                 | 14 (1.1)                                     | 4 (6.0)                                      |
| Type 2 AGN (%)            | 57 <sup>c</sup> (13.2)                  | 100 (15.0)                                 | 23 (1.8)                                     | 0 (0.0)                                      |

<sup>a</sup>Values in parenthesis are percentages of the “Number Classified” (first row)

<sup>b</sup>The 20 probable identifications are excluded here and classified as “Unknown Galaxies”

<sup>c</sup>We declare all these to be probable identifications



Table 3. Type 1 AGN

| Name                    | R.A. <sup>a</sup> | Dec. <sup>a</sup> | $b_J$ | $r_F$  | $K$    | $J - K_s$ | Redshift | ID <sup>b</sup> | Other Name                 |
|-------------------------|-------------------|-------------------|-------|--------|--------|-----------|----------|-----------------|----------------------------|
| 2MASS J00004025-0541009 | 00 00 40.26       | -05 41 00.9       | 17.84 | 16.750 | 13.315 | 2.212     | 0.094    | T1              | 2MASX J00004028-0541012    |
| 2MASS J00020731-4722504 | 00 02 07.32       | -47 22 50.5       | 18.52 | 18.190 | 14.909 | 1.999     | 0.389    | T1              |                            |
| 2MASS J00085227-6233137 | 00 08 52.30       | -62 33 15.3       | 17.27 | 16.530 | 11.825 | 2.252     | 0.184    | T1              | IRAS F00063-6249           |
| 2MASS J00114353-5033299 | 00 11 43.54       | -50 33 30.0       | 18.09 | 16.800 | 13.125 | 2.111     | 0.140    | T1              | 2MASX J00114350-5033302    |
| 2MASS J00163310-0542315 | 00 16 33.10       | -05 42 31.4       | 17.61 | 17.070 | 13.299 | 2.113     | 0.237    | T1              | 1RXS J001633.2-054227      |
| 2MASS J00202646-0254583 | 00 20 26.46       | -02 54 58.2       | 17.97 | 17.680 | 14.951 | 1.889     | 0.363    | T1              |                            |
| 2MASS J00265121-0159238 | 00 26 51.16       | -01 59 23.7       | 19.36 | 17.720 | 15.020 | 2.026     | 0.319    | T1              |                            |
| 2MASS J00315009-3000482 | 00 31 50.08       | -30 00 48.3       | 17.46 | 17.190 | 14.094 | 2.082     | 0.435    | T1              |                            |
| 2MASS J00345758-3221311 | 00 34 57.58       | -32 21 31.2       | 18.77 | 17.590 | 14.303 | 1.997     | 0.186    | T1              | 2dFGRS S440Z049            |
| 2MASS J00470010-1747025 | 00 47 00.05       | -17 47 02.0       | 18.84 | 17.080 | 12.500 | 2.752     | 0.147    | T1              | IRAS 00444-1803            |
| 2MASS J00573811-1406173 | 00 57 38.12       | -14 06 17.3       | 18.56 | 17.780 | 14.458 | 2.219     | 0.207    | T1              |                            |
| 2MASS J00575201-3329048 | 00 57 52.03       | -33 29 04.6       | 18.53 | 17.550 | 14.691 | 2.162     | 0.270    | T1              |                            |
| 2MASS J00593208-1540302 | 00 59 32.11       | -15 40 29.7       | 18.33 | 16.800 | 14.778 | 1.620     | 0.254    | T1              | 1RXS J005932.7-154032      |
| 2MASS J01144251-5136137 | 01 14 42.46       | -51 36 13.8       | 18.71 | 17.970 | 14.806 | 1.746     | 0.205    | T1              |                            |
| 2MASS J01274593-4453170 | 01 27 45.95       | -44 53 17.0       | 17.83 | 17.320 | 14.683 | 1.868     | 0.385    | T1              |                            |
| 2MASS J01283395-2358359 | 01 28 33.96       | -23 58 35.8       | 18.58 | 17.910 | 14.428 | 2.433     | 0.462    | PT1             |                            |
| 2MASS J01290719-2356300 | 01 29 07.24       | -23 56 30.2       | 19.48 | 17.770 | 15.053 | 1.793     | 0.020    | T1              | APMUKS B012644.60-241200.3 |
| 2MASS J01340171-5618454 | 01 34 01.70       | -56 18 45.5       | 17.46 | 17.190 | 13.762 | 2.050     | 0.328    | PT1             | SUMSS J013401-561844       |
| 2MASS J01354636-3539148 | 01 35 46.35       | -35 39 15.3       | 18.03 | 17.050 | 13.396 | 2.000     | 0.137    | T1              | 2MASX J01354638-3539151    |
| 2MASS J01380953-0109201 | 01 38 09.54       | -01 09 20.1       | 16.68 | 16.360 | 13.141 | 2.271     | 0.273    | T1              | SDSS J013809.53-010920.2   |
| 2MASS J01432356-0124523 | 01 43 23.57       | -01 24 52.4       | 18.04 | 17.250 | 13.858 | 2.036     | 0.368    | T1              |                            |
| 2MASS J01553002-0857040 | 01 55 30.03       | -08 57 04.0       | 17.95 | 16.910 | 12.690 | 2.072     | 0.164    | T1              | SDSS J015530.02-085704.0   |
| 2MASS J01593068-1128584 | 01 59 30.69       | -11 28 58.5       | 18.15 | 17.270 | 13.676 | 2.062     | 0.161    | T1              |                            |
| 2MASS J01593518-2010583 | 01 59 35.20       | -20 10 58.4       | 19.15 | 17.670 | 14.078 | 2.267     | 0.317    | PT1             | APMUKS B015713.48-202531.4 |

Table 3—Continued

| Name                    | R.A. <sup>a</sup> | Dec. <sup>a</sup> | $b_J$ | $r_F$  | $K$    | $J - K_s$ | Redshift | ID <sup>b</sup> | Other Name                 |
|-------------------------|-------------------|-------------------|-------|--------|--------|-----------|----------|-----------------|----------------------------|
| 2MASS J02112824-0640013 | 02 11 28.22       | -06 40 00.8       | 18.42 | 18.000 | 14.816 | 2.045     | 0.426    | PT1             |                            |
| 2MASS J02120146-0201539 | 02 12 01.47       | -02 01 53.8       | 19.20 | 17.720 | 14.182 | 2.163     | 0.438    | T1              |                            |
| 2MASS J02144017-6839338 | 02 14 40.21       | -68 39 33.8       | 18.96 | 17.870 | 14.412 | 1.916     | 0.305    | PT1             |                            |
| 2MASS J02155303-4709570 | 02 15 53.04       | -47 09 57.1       | 17.64 | 16.690 | 12.602 | 2.085     | 0.140    | T1              | 2MASX J02155306-4709573    |
| 2MASS J02181461-1012491 | 02 18 14.61       | -10 12 49.1       | 17.86 | 18.170 | 15.054 | 2.036     | 0.568    | PT1             |                            |
| 2MASS J02221945-5332391 | 02 22 19.44       | -53 32 39.1       | 16.61 | 15.540 | 12.626 | 2.035     | 0.095    | T1              |                            |
| 2MASS J02252283-2441528 | 02 25 22.84       | -24 41 52.8       | 17.81 | 17.390 | 14.435 | 2.109     | 0.009    | T1              |                            |
| 2MASS J02254799-1429454 | 02 25 48.01       | -14 29 45.4       | 18.63 | 17.930 | 15.026 | 2.068     | 0.437    | T1              |                            |
| 2MASS J02255003-0601450 | 02 25 50.04       | -06 01 45.1       | 17.13 | 16.380 | 13.574 | 2.156     | 0.319    | T1              |                            |
| 2MASS J02270655-3220448 | 02 27 06.52       | -32 20 44.7       | 18.42 | 17.530 | 14.119 | 1.985     | 0.249    | T1              | 2dFGRS S463Z081            |
| 2MASS J02293513-0552094 | 02 29 35.14       | -05 52 09.4       | 17.47 | 16.940 | 13.928 | 2.280     | 0.293    | T1              |                            |
| 2MASS J02313792-2308312 | 02 31 37.93       | -23 08 31.2       | 15.68 | 15.410 | 12.941 | 2.008     | 0.249    | T1              |                            |
| 2MASS J02331354-1506540 | 02 33 13.55       | -15 06 54.1       | 18.69 | 18.060 | 15.059 | 2.035     | 0.337    | PT1             |                            |
| 2MASS J02365236-5554463 | 02 36 52.33       | -55 54 46.3       | 17.42 | 17.620 | 14.342 | 1.960     | 0.312    | T1              |                            |
| 2MASS J02391868-0115211 | 02 39 18.69       | -01 15 21.1       | 18.52 | 18.150 | 14.919 | 1.975     | 0.374    | T1              | SDSS J023918.70-011521.0   |
| 2MASS J02452486-1623432 | 02 45 24.86       | -16 23 43.3       | 18.81 | 17.660 | 14.252 | 2.034     | 0.286    | T1              | APMUKS B024304.02-163618.0 |
| 2MASS J02460800-1132367 | 02 46 08.01       | -11 32 36.6       | 16.39 | 16.340 | 13.234 | 2.470     | 0.270    | T1              | IRAS F02437-1145           |
| 2MASS J02535862-4558236 | 02 53 58.63       | -45 58 23.9       | 18.87 | 17.970 | 14.189 | 2.837     | 0.460    | PT1             |                            |
| 2MASS J02564173-1231478 | 02 56 41.72       | -12 31 48.4       | 17.27 | 17.110 | 14.926 | 2.034     | 0.473    | T1              |                            |
| 2MASS J02574845-0918443 | 02 57 48.45       | -09 18 44.6       | 18.07 | 17.020 | 13.319 | 2.140     | 0.145    | T1              | 2MASX J02574849-0918440    |
| 2MASS J02593835-1513092 | 02 59 38.35       | -15 13 09.2       | 17.16 | 16.760 | 13.906 | 2.122     | 0.354    | T1              | NVSS J025938-151306        |
| 2MASS J03012933-1632400 | 03 01 29.35       | -16 32 39.8       | 17.00 | 16.940 | 14.150 | 2.110     | 0.334    | T1              |                            |
| 2MASS J03103479-6412052 | 03 10 34.80       | -64 12 05.2       | 17.76 | 16.750 | 13.232 | 1.967     | 0.190    | T1              | 2MASX J03103473-6412054    |
| 2MASS J03153812-0912337 | 03 15 38.11       | -09 12 34.0       | 16.29 | 15.440 | 12.580 | 2.041     | 0.352    | T1              |                            |

Table 3—Continued

| Name                    | R.A. <sup>a</sup> | Dec. <sup>a</sup> | $b_J$ | $r_F$  | $K$    | $J - K_s$ | Redshift | ID <sup>b</sup> | Other Name               |
|-------------------------|-------------------|-------------------|-------|--------|--------|-----------|----------|-----------------|--------------------------|
| 2MASS J03173580-3817251 | 03 17 35.81       | -38 17 25.3       | 18.21 | 17.840 | 14.693 | 2.290     | 0.254    | T1              |                          |
| 2MASS J03232133-2557442 | 03 23 21.34       | -25 57 44.3       | 17.73 | 17.530 | 14.568 | 2.232     | 0.290    | T1              |                          |
| 2MASS J03261346-2018137 | 03 26 13.45       | -20 18 13.7       | 18.41 | 17.760 | 14.582 | 2.139     | 0.281    | PT1             |                          |
| 2MASS J03360954-0619128 | 03 36 09.52       | -06 19 12.9       | 17.99 | 18.420 | 15.181 | 1.662     | 0.438    | T1              | SDSS J033609.54-061913.1 |
| 2MASS J03374281-2522095 | 03 37 42.81       | -25 22 09.5       | 17.41 | 16.910 | 13.660 | 2.270     | 0.273    | T1              |                          |
| 2MASS J03412733-0906436 | 03 41 27.33       | -09 06 43.5       | 16.99 | 16.330 | 13.554 | 1.997     | 0.383    | T1              |                          |
| 2MASS J03413408-0547154 | 03 41 34.11       | -05 47 15.4       | 18.37 | 17.170 | 14.595 | 2.007     | 0.137    | T1              | SDSS J034134.07-054715.7 |
| 2MASS J03440463-1252226 | 03 44 04.62       | -12 52 22.6       | 17.93 | 16.700 | 13.001 | 2.230     | 0.093    | T1              | 2MASX J03440465-1252222  |
| 2MASS J03561630-1237095 | 03 56 16.33       | -12 37 09.2       | 17.50 | 17.550 | 14.828 | 1.955     | 0.318    | T1              | 1RXS J035616.4-123712    |
| 2MASS J03561996-6251391 | 03 56 19.96       | -62 51 39.1       | 18.16 | 17.270 | 12.617 | 2.948     | 0.108    | T1              | 2MASX J03561995-6251391  |
| 2MASS J04023421-3152594 | 04 02 34.22       | -31 52 59.2       | 17.86 | 17.030 | 13.963 | 2.085     | 0.297    | PT1             | NVSS J040234-315301      |
| 2MASS J04043381-4039545 | 04 04 33.81       | -40 39 54.6       | 18.65 | 17.860 | 14.525 | 2.006     | 0.623    | T1              |                          |
| 2MASS J04170175-0309594 | 04 17 01.74       | -03 09 59.7       | 18.53 | 17.580 | 14.745 | 2.214     | 0.330    | T1              |                          |
| 2MASS J04225656-1854422 | 04 22 56.56       | -18 54 42.3       | 16.89 | 14.410 | 11.605 | 2.209     | 0.064    | T1              | 2MASX J04225654-1854424  |
| 2MASS J04243795-2318335 | 04 24 37.96       | -23 18 33.6       | 18.14 | 17.350 | 14.621 | 2.009     | 0.542    | T1              |                          |
| 2MASS J04324870-0921117 | 04 32 48.70       | -09 21 11.6       | 18.58 | 17.690 | 14.000 | 2.133     | 0.216    | T1              |                          |
| 2MASS J04332250-1422287 | 04 33 22.51       | -14 22 28.6       | 17.42 | 16.800 | 13.592 | 2.276     | 0.347    | T1              | 1WGA J0433.3-1422        |
| 2MASS J04352649-1643460 | 04 35 26.50       | -16 43 46.0       | 17.30 | 16.310 | 13.828 | 2.031     | 0.098    | T1              |                          |
| 2MASS J04360031-0405540 | 04 36 00.32       | -04 05 54.0       | 18.15 | 17.830 | 14.492 | 2.235     | 0.091    | T1              |                          |
| 2MASS J04364839-1123559 | 04 36 48.40       | -11 23 55.9       | 17.38 | 16.770 | 13.720 | 2.129     | 0.207    | T1              | NVSS J043647-112347      |
| 2MASS J04411070-0639383 | 04 41 10.71       | -06 39 38.3       | 18.73 | 17.430 | 14.706 | 2.241     | 0.312    | T1              |                          |
| 2MASS J04433082-3508499 | 04 43 30.78       | -35 08 49.9       | 18.24 | 17.970 | 14.553 | 2.049     | 0.457    | T1              |                          |
| 2MASS J04481925-2158473 | 04 48 19.25       | -21 58 47.1       | 18.57 | 17.400 | 13.408 | 2.209     | 0.111    | T1              | 2MASX J04481922-2158468  |
| 2MASS J05022413-3546422 | 05 02 24.15       | -35 46 42.3       | 18.34 | 17.950 | 14.417 | 1.993     | 0.155    | T1              |                          |

Table 3—Continued

| Name                    | R.A. <sup>a</sup> | Dec. <sup>a</sup> | $b_J$ | $r_F$  | $K$    | $J - K_s$ | Redshift | ID <sup>b</sup> | Other Name                 |
|-------------------------|-------------------|-------------------|-------|--------|--------|-----------|----------|-----------------|----------------------------|
| 2MASS J05043443-1521193 | 05 04 34.42       | -15 21 19.3       | 17.21 | 16.760 | 13.768 | 2.200     | 0.390    | T1              |                            |
| 2MASS J05063975-3416422 | 05 06 39.77       | -34 16 42.2       | 18.96 | 17.480 | 14.211 | 1.990     | 0.173    | T1              | APMUKS B050450.33-342037.7 |
| 2MASS J05222203-4524370 | 05 22 21.99       | -45 24 36.8       | 17.73 | 17.390 | 13.296 | 2.112     | 0.172    | T1              | 1WGA J0522.3-4524          |
| 2MASS J05372445-3817586 | 05 37 24.48       | -38 17 58.7       | 18.02 | 17.300 | 14.517 | 2.023     | 0.332    | T1              |                            |
| 2MASS J10012986-0338334 | 10 01 29.88       | -03 38 33.5       | 17.75 | 17.090 | 14.280 | 2.038     | 1.389    | PT1             |                            |
| 2MASS J10264404-0425408 | 10 26 44.05       | -04 25 40.6       | 16.99 | 16.930 | 14.539 | 2.007     | 0.254    | T1              |                            |
| 2MASS J10443748-0705162 | 10 44 37.49       | -07 05 15.9       | 17.25 | 17.340 | 14.163 | 2.085     | 0.301    | PT1             |                            |
| 2MASS J11291836-2855531 | 11 29 18.36       | -28 55 53.1       | 18.87 | 18.050 | 14.604 | 2.066     | 0.192    | T1              |                            |
| 2MASS J11294994-1153488 | 11 29 49.93       | -11 53 49.4       | 17.95 | 17.720 | 15.068 | 1.721     | 0.431    | T1              |                            |
| 2MASS J12101994-1157105 | 12 10 19.91       | -11 57 10.4       | 16.80 | 16.950 | 13.544 | 2.111     | 0.206    | T1              | LCRS B120745.5-114029      |
| 2MASS J12140669-2948164 | 12 14 06.69       | -29 48 16.4       | 17.66 | 17.430 | 14.658 | 2.053     | 0.498    | T1              |                            |
| 2MASS J12154013-2350122 | 12 15 40.14       | -23 50 12.2       | 18.89 | 17.420 | 14.015 | 2.001     | 0.232    | T1              | 2MASX J12154013-2350126    |
| 2MASS J12524011-3036579 | 12 52 40.12       | -30 36 58.0       | 18.75 | 18.350 | 15.278 | 1.962     | 0.430    | PT1             |                            |
| 2MASS J12590021-3152245 | 12 59 00.21       | -31 52 24.5       | 18.66 | 18.080 | 14.090 | 2.327     | 0.292    | T1              |                            |
| 2MASS J13210070-0806482 | 13 21 00.72       | -08 06 47.9       | 17.88 | 17.560 | 14.786 | 2.074     | 0.507    | T1              |                            |
| 2MASS J13240925-1525097 | 13 24 09.26       | -15 25 09.4       | 17.69 | 17.320 | 14.754 | 1.917     | 0.531    | PT1             |                            |
| 2MASS J13265209-1506385 | 13 26 52.11       | -15 06 38.8       | 19.94 | 17.880 | 13.872 | 2.144     | 0.323    | T1              |                            |
| 2MASS J13450643-2705409 | 13 45 06.44       | -27 05 41.0       | 18.22 | 17.640 | 14.783 | 1.950     | 0.276    | T1              |                            |
| 2MASS J13500251-2619308 | 13 50 02.52       | -26 19 30.8       | 18.46 | 17.010 | 14.133 | 2.006     | 0.208    | T1              | 2MASX J13500249-2619306    |
| 2MASS J14403905-1927129 | 14 40 39.05       | -19 27 13.0       | 18.21 | 17.400 | 14.264 | 2.251     | 0.295    | T1              |                            |
| 2MASS J15400255-1451363 | 15 40 02.54       | -14 51 36.3       | 19.03 | 17.670 | 14.783 | 1.868     | 0.193    | T1              |                            |
| 2MASS J15470139-0632099 | 15 47 01.41       | -06 32 09.9       | 18.34 | 17.420 | 14.127 | 2.048     | 0.252    | T1              |                            |
| 2MASS J15475594-0610480 | 15 47 55.95       | -06 10 48.3       | 18.29 | 17.460 | 14.539 | 1.877     | 0.129    | T1              |                            |
| 2MASS J20202833-3014140 | 20 20 28.33       | -30 14 14.2       | 19.63 | 17.930 | 13.939 | 2.204     | 0.196    | T1              |                            |

Table 3—Continued

| Name                    | R.A. <sup>a</sup> | Dec. <sup>a</sup> | $b_J$ | $r_F$  | $K$    | $J - K_s$ | Redshift | ID <sup>b</sup> | Other Name              |
|-------------------------|-------------------|-------------------|-------|--------|--------|-----------|----------|-----------------|-------------------------|
| 2MASS J20223079-3236086 | 20 22 30.79       | -32 36 08.6       | 17.45 | 16.950 | 13.069 | 2.030     | 0.142    | T1              |                         |
| 2MASS J20331662-2253169 | 20 33 16.62       | -22 53 17.0       | 18.59 | 17.330 | 13.467 | 2.109     | 0.131    | T1              | PKS 2030-23             |
| 2MASS J20344129-5126573 | 20 34 41.28       | -51 26 57.3       | 17.81 | 16.400 | 12.772 | 2.024     | 0.128    | T1              | 2MASX J20344130-5126572 |
| 2MASS J20345400-3131563 | 20 34 53.99       | -31 31 56.4       | 18.35 | 17.310 | 14.332 | 1.842     | 0.202    | T1              |                         |
| 2MASS J20400728-5237227 | 20 40 07.30       | -52 37 22.6       | 17.00 | 15.980 | 12.532 | 2.325     | 0.128    | T1              | 2MASX J20400731-5237224 |
| 2MASS J20465715-7400040 | 20 46 57.15       | -74 00 04.1       | 17.46 | 17.680 | 14.345 | 2.189     | 0.526    | T1              | PKS 2041-741            |
| 2MASS J20585386-2409418 | 20 58 53.86       | -24 09 41.8       | 19.10 | 17.700 | 14.212 | 2.038     | 0.294    | PT1             |                         |
| 2MASS J21071766-5503097 | 21 07 17.66       | -55 03 10.1       | 18.60 | 18.010 | 14.117 | 2.374     | 0.461    | PT1             | SUMSS J210717-550308    |
| 2MASS J21132600-6316184 | 21 13 26.04       | -63 16 18.4       | 18.49 | 17.780 | 14.172 | 2.075     | 0.255    | T1              |                         |
| 2MASS J21133234-6257134 | 21 13 32.35       | -62 57 13.5       | 17.67 | 17.010 | 13.545 | 2.066     | 0.168    | T1              |                         |
| 2MASS J21260042-2558396 | 21 26 00.42       | -25 58 39.6       | 18.73 | 17.900 | 14.894 | 1.873     | 0.343    | T1              |                         |
| 2MASS J21333132-6120301 | 21 33 31.31       | -61 20 30.2       | 18.32 | 17.590 | 13.840 | 2.062     | 0.116    | T1              |                         |
| 2MASS J21570360-7322204 | 21 57 03.61       | -73 22 20.5       | 17.82 | 16.640 | 13.033 | 1.967     | 0.096    | T1              | 2MASX J21570361-7322205 |
| 2MASS J21571362-4201497 | 21 57 13.61       | -42 01 49.2       | 18.64 | 17.910 | 14.562 | 1.888     | 1.321    | T1              | LCRS B215408.7-421607   |
| 2MASS J21572015-4036138 | 21 57 20.17       | -40 36 13.8       | 17.77 | 17.820 | 14.058 | 2.359     | 0.301    | T1              |                         |
| 2MASS J21572316-3123064 | 21 57 23.17       | -31 23 06.5       | 16.50 | 15.640 | 12.469 | 2.151     | 0.085    | T1              | 1RXS J215723.3-31230    |
| 2MASS J22161121-3947337 | 22 16 11.23       | -39 47 33.7       | 18.35 | 16.500 | 13.920 | 2.004     | 0.246    | T1              |                         |
| 2MASS J22165321-4451568 | 22 16 53.21       | -44 51 57.0       | 15.83 | 15.340 | 12.421 | 2.067     | 0.135    | T1              | LCRS B221349.8-450657   |
| 2MASS J22170559-3619460 | 22 17 05.60       | -36 19 46.1       | 17.58 | 17.120 | 13.687 | 2.040     | 0.151    | T1              |                         |
| 2MASS J22180018-3957228 | 22 18 00.19       | -39 57 22.7       | 17.83 | 16.640 | 13.177 | 2.072     | 0.244    | T1              |                         |
| 2MASS J22212645-4757598 | 22 21 26.46       | -47 57 59.6       | 17.97 | 17.970 | 14.520 | 1.969     | 0.198    | T1              |                         |
| 2MASS J22250207-1841401 | 22 25 02.09       | -18 41 40.0       | 17.50 | 17.540 | 14.573 | 2.080     | 0.302    | T1              |                         |
| 2MASS J22253449-1939566 | 22 25 34.50       | -19 39 56.6       | 19.38 | 17.910 | 14.805 | 2.253     | 0.364    | PT1             |                         |
| 2MASS J22385748-0539206 | 22 38 57.49       | -05 39 20.6       | 18.62 | 16.750 | 13.425 | 2.130     | 0.174    | T1              | 1WGA J2238.9-0539       |

Table 3—Continued

| Name                    | R.A. <sup>a</sup> | Dec. <sup>a</sup> | $b_J$ | $r_F$  | $K$    | $J - K_s$ | Redshift | ID <sup>b</sup> | Other Name                 |
|-------------------------|-------------------|-------------------|-------|--------|--------|-----------|----------|-----------------|----------------------------|
| 2MASS J22423001-2745299 | 22 42 30.02       | -27 45 29.6       | 19.58 | 17.740 | 14.773 | 1.695     | 0.199    | T1              |                            |
| 2MASS J22431660-2020570 | 22 43 16.59       | -20 20 57.1       | 18.19 | 17.990 | 14.849 | 2.202     | 0.276    | T1              |                            |
| 2MASS J22433493-3928397 | 22 43 34.94       | -39 28 39.6       | 19.10 | 17.630 | 14.025 | 2.042     | 0.217    | T1              | APMUKS B224042.73-394424.8 |
| 2MASS J22553836-0245335 | 22 55 38.34       | -02 45 33.1       | 18.48 | 17.730 | 14.764 | 1.812     | 0.273    | T1              | 1WGA J2255.6-0245          |
| 2MASS J22573178-0651513 | 22 57 31.79       | -06 51 51.2       | 17.42 | 17.370 | 14.731 | 1.926     | 0.317    | T1              |                            |
| 2MASS J23054834-0314121 | 23 05 48.29       | -03 14 11.7       | 18.59 | 17.810 | 14.175 | 2.600     | 0.318    | T1              |                            |
| 2MASS J23062901-4951453 | 23 06 29.01       | -49 51 45.3       | 18.12 | 17.670 | 14.417 | 1.962     | 0.118    | T1              |                            |
| 2MASS J23180937-1125452 | 23 18 09.36       | -11 25 45.5       | 17.49 | 17.230 | 14.745 | 1.866     | 0.042    | T1              |                            |
| 2MASS J23253138-3010560 | 23 25 31.39       | -30 10 56.1       | 19.29 | 15.010 | 10.999 | 2.447     | 0.417    | PT1             |                            |
| 2MASS J23305477-0956480 | 23 30 54.78       | -09 56 48.1       | 18.35 | 17.630 | 14.190 | 1.997     | 0.250    | T1              | 2MASX J23305473-0956479    |
| 2MASS J23342108-1421319 | 23 34 21.12       | -14 21 31.3       | 16.67 | 17.020 | 13.971 | 1.861     | 0.243    | T1              | 1RXS J233421.6-142128      |
| 2MASS J23352324-3945052 | 23 35 23.26       | -39 45 05.2       | 18.40 | 17.770 | 14.884 | 1.960     | 0.019    | T1              |                            |
| 2MASS J23430906-5412369 | 23 43 09.09       | -54 12 36.8       | 17.81 | 18.230 | 14.609 | 2.189     | 0.624    | PT1             | SUMSS J234308-541238       |
| 2MASS J23441698-3322367 | 23 44 16.95       | -33 22 36.4       | 18.97 | 18.120 | 14.693 | 2.312     | 0.233    | T1              |                            |
| 2MASS J23524661-2116467 | 23 52 46.60       | -21 16 46.9       | 17.30 | 17.120 | 14.751 | 1.937     | 0.280    | T1              | 1RXS J235247.1-211644      |
| 2MASS J23582823-2259320 | 23 58 28.22       | -22 59 31.9       | 18.09 | 16.230 | 13.415 | 2.006     | 0.114    | PT1             | 2MASX J23582823-2259322    |

<sup>a</sup>In J2000.0, units are hours, minutes, seconds for R.A., and degrees, arcminutes, arcseconds for Dec.

<sup>b</sup>T1 = securely identified type 1 AGN; PT1 = probable identification

Table 4. Type 2 AGN<sup>a</sup>

| Name                    | R.A. <sup>b</sup> | Dec. <sup>b</sup> | $b_J$ | $r_F$  | $K$    | $J - K_s$ | Redshift | Other Name                 |
|-------------------------|-------------------|-------------------|-------|--------|--------|-----------|----------|----------------------------|
| 2MASS J00041584-4938500 | 00 04 15.83       | -49 38 50.2       | 18.75 | 17.420 | 14.399 | 1.776     | 0.199    | 2MASX J00041588-4938507    |
| 2MASS J00112456-0808506 | 00 11 24.57       | -08 08 50.6       | 19.92 | 17.560 | 14.775 | 2.069     | 0.136    | APMUKS B000851.08-08252    |
| 2MASS J00153042-0750548 | 00 15 30.43       | -07 50 54.7       | 19.27 | 17.780 | 14.217 | 2.080     | 0.178    | 2MASX J00153041-0750549    |
| 2MASS J00213743-3726445 | 00 21 37.41       | -37 26 44.8       | 18.75 | 17.450 | 14.304 | 2.254     | 0.197    |                            |
| 2MASS J00240550-1540006 | 00 24 05.51       | -15 40 00.4       | 19.07 | 17.680 | 13.926 | 2.099     | 0.241    | NVSS J002405-154004        |
| 2MASS J01023200-2151264 | 01 02 31.99       | -21 51 26.6       | 12.24 | 14.830 | 14.890 | 1.065     | 0.040    | 2MASX J01023199-2151267    |
| 2MASS J01220424-5355324 | 01 22 04.19       | -53 55 33.1       | 18.89 | 17.710 | 14.606 | 2.006     | 0.316    | APMUKS B012002.43-541113.6 |
| 2MASS J01231824-2207033 | 01 23 18.25       | -22 07 03.2       | 19.55 | 17.830 | 14.031 | 2.060     | 0.388    |                            |
| 2MASS J01265229-4556045 | 01 26 52.28       | -45 56 04.5       | 19.77 | 17.810 | 14.903 | 1.508     | 0.294    | IRAS F01247-4611           |
| 2MASS J01291045-4331345 | 01 29 10.46       | -43 31 34.6       | 20.26 | 17.830 | 14.823 | 2.003     | 0.282    |                            |
| 2MASS J01413624-1747177 | 01 41 36.25       | -17 47 17.6       | 17.83 | 17.260 | 14.477 | 1.795     | 0.311    |                            |
| 2MASS J02171791-2638482 | 02 17 17.90       | -26 38 48.3       | 19.16 | 17.900 | 14.775 | 2.140     | 0.201    |                            |
| 2MASS J02333333-0635397 | 02 33 33.33       | -06 35 39.5       | 19.10 | 17.570 | 14.403 | 2.051     | 0.185    |                            |
| 2MASS J02340157-1934369 | 02 34 01.59       | -19 34 37.1       | 17.96 | 17.730 | 15.105 | 1.932     | 0.346    |                            |
| 2MASS J02345773-3349442 | 02 34 57.73       | -33 49 44.4       | 18.37 | 16.580 | 14.802 | 1.756     | 0.117    | 2dFGRS S518Z006            |
| 2MASS J03143680-0557035 | 03 14 36.79       | -05 57 03.2       | 18.15 | 17.520 | 14.739 | 2.124     | 0.107    | APMUKS B031208.24-060810.4 |
| 2MASS J03232591-2110586 | 03 23 25.90       | -21 10 58.7       | 19.41 | 17.970 | 14.648 | 1.989     | 0.352    |                            |
| 2MASS J03340366-1454428 | 03 34 03.66       | -14 54 43.0       | 18.63 | 17.670 | 13.928 | 1.967     | 0.167    | APMUKS B033144.22-150442.8 |
| 2MASS J03474693-2424458 | 03 47 46.90       | -24 24 45.8       | 18.59 | 18.160 | 15.214 | 1.674     | 0.272    |                            |
| 2MASS J03535649-1605395 | 03 53 56.48       | -16 05 39.9       | 19.90 | 17.390 | 15.057 | 1.964     | 0.066    |                            |
| 2MASS J04043951-0930307 | 04 04 39.52       | -09 30 30.7       | 18.75 | 17.160 | 14.952 | 2.402     | 0.359    |                            |
| 2MASS J04082380-2152363 | 04 08 23.81       | -21 52 36.3       | 19.93 | 17.600 | 13.498 | 2.636     | 0.207    |                            |
| 2MASS J04192642-0600032 | 04 19 26.42       | -06 00 03.3       | 19.06 | 17.880 | 14.601 | 1.952     | 0.223    |                            |
| 2MASS J04221665-2315307 | 04 22 16.65       | -23 15 30.9       | 18.96 | 18.100 | 14.758 | 1.914     | 0.156    | APMUKS B042009.08-232228.6 |

Table 4—Continued

| Name                    | R.A. <sup>b</sup> | Dec. <sup>b</sup> | $b_J$ | $r_F$  | $K$    | $J - K_s$ | Redshift | Other Name               |
|-------------------------|-------------------|-------------------|-------|--------|--------|-----------|----------|--------------------------|
| 2MASS J04242530-3604244 | 04 24 25.30       | -36 04 24.6       | 18.35 | 17.210 | 13.047 | 2.825     | 0.150    | IRAS F04226-3611         |
| 2MASS J04402018-0802175 | 04 40 20.18       | -08 02 17.4       | 19.32 | 17.960 | 13.916 | 2.070     | 0.189    | 2MASX J04402018-0802174  |
| 2MASS J04473869-4124594 | 04 47 38.70       | -41 24 59.4       | 19.04 | 17.380 | 13.550 | 2.003     | 0.226    | 2MASX J04473873-4124592  |
| 2MASS J04545129-3513006 | 04 54 51.28       | -35 13 00.9       | 19.29 | 17.860 | 14.256 | 2.208     | 0.240    |                          |
| 2MASS J04562039-1701279 | 04 56 20.41       | -17 01 28.0       | 18.54 | 17.500 | 14.188 | 1.941     | 0.188    |                          |
| 2MASS J04570851-2415069 | 04 57 08.53       | -24 15 06.7       | 19.30 | 17.760 | 14.445 | 2.518     | 0.360    |                          |
| 2MASS J05003208-6032458 | 05 00 32.09       | -60 32 45.8       | 19.67 | 17.650 | 14.153 | 2.216     | 0.317    |                          |
| 2MASS J05015803-2604343 | 05 01 58.04       | -26 04 34.2       | 17.21 | 16.630 | 14.043 | 2.007     | 0.037    | 2MASX J05015805-2604341  |
| 2MASS J05142233-2227103 | 05 14 22.32       | -22 27 10.4       | 18.41 | 17.930 | 15.160 | 1.966     | 0.357    |                          |
| 2MASS J05302635-3452048 | 05 30 26.35       | -34 52 04.9       | 19.28 | 17.350 | 12.922 | 2.307     | 0.298    | NVSS J053026-345207      |
| 2MASS J05513207-5655295 | 05 51 32.04       | -56 55 29.5       | 19.17 | 17.660 | 13.908 | 2.140     | 0.257    | PKS 0550-569             |
| 2MASS J09490740-1211328 | 09 49 07.42       | -12 11 32.8       | 17.81 | 17.250 | 13.624 | 2.323     | 0.093    |                          |
| 2MASS J10505072-1000060 | 10 50 50.71       | -10 00 05.9       | 18.53 | 17.570 | 14.223 | 2.123     | 0.193    | NVSS J105050-100001      |
| 2MASS J11072722-0125110 | 11 07 27.22       | -01 25 11.0       | 18.63 | 17.520 | 14.135 | 1.894     | 0.169    | 2MASX J11072722-0125117  |
| 2MASS J11575615-0453498 | 11 57 56.19       | -04 53 49.4       | 19.03 | 17.760 | 15.378 | 1.513     | 0.190    |                          |
| 2MASS J12294408-1009001 | 12 29 44.07       | -10 09 00.2       | 19.71 | 17.950 | 14.224 | 2.323     | 0.268    | NVSS J122944-100900      |
| 2MASS J13021118-1201264 | 13 02 11.17       | -12 01 26.6       | 18.56 | 17.320 | 14.061 | 2.450     | 0.191    | 2MASX J13021117-1201265  |
| 2MASS J14144317-1556194 | 14 14 43.16       | -15 56 19.3       | 19.57 | 17.960 | 14.370 | 1.904     | 0.212    |                          |
| 2MASS J14255845-1553274 | 14 25 58.46       | -15 53 27.5       | 19.37 | 17.940 | 14.377 | 2.235     | 0.284    |                          |
| 2MASS J14495686-0301555 | 14 49 56.88       | -03 01 55.6       | 18.68 | 17.580 | 14.481 | 2.085     | 0.246    | LCRS B144720.8-024932    |
| 2MASS J15250421-0111569 | 15 25 04.23       | -01 11 57.2       | 18.66 | 17.750 | 14.799 | 2.048     | 0.123    | SDSS J152504.19-011156.5 |
| 2MASS J15320140-0858124 | 15 32 01.40       | -08 58 12.4       | 19.25 | 17.970 | 14.694 | 2.077     | 0.157    |                          |
| 2MASS J20473227-4841084 | 20 47 32.27       | -48 41 08.5       | 18.32 | 16.920 | 13.682 | 2.163     | 0.145    | 2MASX J20473225-4841082  |
| 2MASS J21011126-2143329 | 21 01 11.26       | -21 43 33.1       | 18.21 | 17.530 | 13.698 | 2.065     | 0.304    |                          |



Table 4—Continued

| Name                    | R.A. <sup>b</sup> | Dec. <sup>b</sup> | $b_J$ | $r_F$  | $K$    | $J - K_s$ | Redshift | Other Name                 |
|-------------------------|-------------------|-------------------|-------|--------|--------|-----------|----------|----------------------------|
| 2MASS J21291755-6238414 | 21 29 17.55       | -62 38 41.4       | 18.94 | 18.090 | 15.003 | 2.037     | 0.232    | APMUKS B212523.73-625150.2 |
| 2MASS J21300805-0155571 | 21 30 08.05       | -01 55 57.1       | 19.75 | 17.950 | 14.793 | 2.107     | 0.290    | RX J2130.2-0156            |
| 2MASS J21381991-1001522 | 21 38 19.93       | -10 01 52.2       | 18.72 | 17.530 | 14.174 | 1.958     | 0.206    | 2MASX J21381993-1001522    |
| 2MASS J21454002-2919369 | 21 45 40.02       | -29 19 36.9       | 19.44 | 17.410 | 14.094 | 2.009     | 0.341    | APMUKS B214245.16-293329.4 |
| 2MASS J21462665-4212558 | 21 46 26.65       | -42 12 56.1       | 18.96 | 17.830 | 15.181 | 1.877     | 0.209    |                            |
| 2MASS J22024635-1055517 | 22 02 46.36       | -10 55 51.0       | 18.83 | 17.430 | 12.847 | 2.526     | 0.238    | APMUKS B220006.09-111022.8 |
| 2MASS J22060976-3558119 | 22 06 09.70       | -35 58 12.1       | 20.20 | 17.980 | 14.999 | 1.702     | 0.056    |                            |
| 2MASS J23200024-4309095 | 23 20 00.23       | -43 09 09.5       | 19.01 | 17.670 | 14.096 | 2.054     | 0.177    | 2MASX J23200025-4309100    |
| 2MASS J23572052-5503091 | 23 57 20.53       | -55 03 09.3       | 19.23 | 17.720 | 14.809 | 1.989     | 0.300    |                            |

<sup>a</sup>All these are *probable* identifications (See section 4.1)

<sup>b</sup>In J2000.0, units are hours, minutes, seconds for R.A., and degrees, arcminutes, arcseconds for Dec.